

# Compatible Repair Mortars: A New Methodology Based on Digital Image Analysis Applied to the Casemates of Algiers

M. Akouche, A. Lico, S. Rescic, R. Grazzini, G. Misseri, N. Abderrahim Mahindad & L. Rovero

To cite this article: M. Akouche, A. Lico, S. Rescic, R. Grazzini, G. Misseri, N. Abderrahim Mahindad & L. Rovero (27 Apr 2025): Compatible Repair Mortars: A New Methodology Based on Digital Image Analysis Applied to the Casemates of Algiers, International Journal of Architectural Heritage, DOI: [10.1080/15583058.2025.2487526](https://doi.org/10.1080/15583058.2025.2487526)

To link to this article: <https://doi.org/10.1080/15583058.2025.2487526>



Published online: 27 Apr 2025.



Submit your article to this journal [↗](#)



Article views: 1



View related articles [↗](#)



View Crossmark data [↗](#)



# Compatible Repair Mortars: A New Methodology Based on Digital Image Analysis Applied to the Casemates of Algiers

M. Akouche<sup>a,b</sup>, A. Lico<sup>a</sup>, S. Rescic<sup>c</sup>, R. Grazzini<sup>a</sup>, G. Misseri<sup>a</sup>, N. Abderrahim Mahindad<sup>b</sup>, and L. Rovero<sup>a</sup>

<sup>a</sup>Materials and Structures division - Department of Architecture, University of Florence, Florence, Italy; <sup>b</sup>Environment and Technology for Architecture and Heritage (ETAP), Institute of Architecture and Urbanism, University of Blida1, Blida, Algeria; <sup>c</sup>Institute of Cultural Heritage Sciences - National Research Council, Florence, Italy

## ABSTRACT

A methodology based on systematizing information gained from characterization tests on original mortars and quantifying acceptance criteria is proposed to define repair mortars complying with the compatibility principle's requirements. To this aim, results from physical and mechanical tests combined with optical-microscope Digital Image Analysis (DIA) of thin sections of mortars observed under polarized light are employed to define the original mortar characteristics efficiently and rigorously. Then, compatibility acceptance criteria, including prescriptions on porosity, bulk density, and compressive strength, are defined for the new mortar. The allowable variations of these parameters are quantified to assess to what extent the new mortar is similar to, i.e. compatible with, the original one. An iterative procedure to correct the mix design is proposed based on the comparison between the new and the original mortar. The mortars sampled from the Ottoman military building Casemates located in the Casbah of Algiers are employed as case study.

## ARTICLE HISTORY

Received 1 October 2024  
Accepted 22 March 2025

## KEYWORDS

compatibility principle;  
conservation; digital imaging  
analysis; lime mortar; mix  
design; penetrometric test;  
thin section

## 1. Introduction

Among the conservation actions on historic buildings, the use of selected specific mortars is essential for many types of structural measures, as the insertion of missing masonry parts and repointing bedding joints, to mention the most common cases (Groot et al. 2022; Groot, Ashall, and Hughes 2007; Henriques 2005; ICOMOS 2003; Iscarsah 2005; Luque, Cultrone, and Sebastián 2010; Moropoulou, Bakolas, and Bisbikou 2000; 2012; Schafer and Hilsdorf 1993; Van Balen et al. 2005). Even in the implementation of compatible anti-seismic systems based on sheets of fiber-reinforced composites, mortars acting as matrices are pivotal since they adhere to the wall surface and transfer the actions to the fiber reinforcement (Drdácký and Michoinova 2003; Fazzi, Misseri, and Rovero 2023; Misseri, Rovero, and Galassi 2021; Rovero, Galassi, and Misseri 2020).

The selection of such mortars is a critical point in the design of conservation measures for historical buildings if conservation criteria, based on ICOMOS principles, are correctly considered (Apostolopoulou et al. 2020; Avdelidis and Moropoulou 2004; Baccaro et al. 2000; Beck and Al-Mukhtar 2008; Bocca and Grazzini 2012, 2013; Charter 1964; Dimitrova et al. 2020; Elert et al. 2002; Grammatikakis et al. 2015; Groot, Ashall, and Hughes 2007; Iscarsah 2005; Moropoulou et al. 2013;

Rodrigues and Grossi 2007; Schueremans et al. 2011; Szemerey-Kiss and Török 2017; Zerbinatti et al. 2018). From this perspective, the repair mortars must be compatible, on a physical-chemical and mechanical level, with the existing ones.

Reversibility is another vital conservation requirement to ensure that the mortar can be removed mechanically without damaging the underlying masonry. Besides that, the mortars must not limit the breathability of the masonry, causing problems resulting from rising dampness and preventing salts migration (Houck and Scherer 2006; Granneman, Lubelli, and van Hees 2019a; Bracciale et al. 2020). Recently, sustainability concerns have driven research on new conservation materials (Apostolopoulou et al. 2018; Bertolin and Loli 2018; Dimitrova et al. 2020; Do Rosario Veiga et al. 2010), adding to methodologies to improve workability, durability, and mechanical resistance (Drougkas et al. 2023) through the inclusion of various fillers with the ability to modify the mortar microstructure (Bekzhanova, Ali Memon, and Ryeol Kim 2021; Birgin et al. 2021; Dalla et al. 2021; Del Mar Barbero-Barrera et al. 2014; Drougkas et al. 2023; Faria et al. 2017; Restuccia et al. 2018; Wang and Aslani 2022).

The great variety of mortars used over the centuries depends on their function and the local building culture,

an expression of the place and the historical period. The use of lime as a binder for mortars dates back to the prehistoric period when its production was accidental. The hydraulic lime mortars appear during the Phoenician period (Pecchioni et al. 2008). Several factors influence the quality of traditional lime, such as the structure of the limestone, particularly the porosity, the cooking temperature and duration, and the possible presence of impurities in the limestone. Throughout history, hydraulic properties have been obtained by the addition of materials such as pozzolana or bricks and ceramic products, called “cocciopesto”, rich in silica and alumina, which combine with calcium (Gomes, Roberto Lopes Lima, and Vianna Fontes 2012), which also offer strength increase (Chen et al. 2024; Degryse, Elsen, and Waelkens 2002). Unlike air lime, which hardens through carbonation by reacting with atmospheric carbon dioxide, hydraulic lime also hardens through reaction with water, making it more suitable for environments exposed to moisture (Matias, Torres, and Faria 2016). The different composition and setting conditions in hydraulic mortars affect primary porosity, which is made by peculiarly shaped pores and is lower compared to air lime mortars (Thomson et al. 2004). The strength of air lime mortars is up to 7 times lower than that of hydraulic lime mortars (Lanas et al. 2004).

The binder-aggregate ratio ( $b/a$ ), the water-binder ratio ( $w/b$ ), the curing time, the grain size distribution and the nature and geometry of the aggregates are crucial factors affecting mortar characteristics. The greater the  $b/a$  ratio, up to 2:1, the greater the compressive strength, which increases remarkably with increasing curing time (Costigan and Pavia 2009; Drougkas, Roca, and Molins 2016; Kalagri, Karatasios, and Kilikoglou 2014; Moropoulou et al. 2005); strength increase in time is slower for richer mortars (Lanas and Alvarez-Galindo 2003), and in the long-term-curing, three phases can be identified (Lanas et al. 2004). The greater the amount of water, the better the workability of the fresh mortar (Garijo et al. 2017), but the lower the strength. For fixed  $b/a$ , the greater the maximum size of the aggregate, the less water needed and hence the more significant the strength (Kalagri, Karatasios, and Kilikoglou 2014; Stefanidou and Papayianni 2005). For fixed  $b/a$  and  $w/b$  ratios, finer grain-size distributions, but still well graded, provide greater strength (Degryse, Elsen, and Waelkens 2002; Lanas and Alvarez-Galindo 2003), indeed coarse aggregate might increase mortar deformability. Calcite sands can improve the mortar strength for the close chemical similarity with binder (Cazalla Vázquez 2002; Gleize, Müller, and Roman 2003; Heikal, El-Didamony, and Morsy 2000; Lanas and Alvarez-Galindo 2003; Lanas

et al. 2004) and for similar granulometry and aggregate nature, a rounded shape of grains slightly reduces strength (Cazalla Vázquez 2002; Kalagri, Karatasios, and Kilikoglou 2014; Lanas et al. 2004). Porosity reduces with aggregate increase since adequate packing of grains develops (Kalagri, Karatasios, and Kilikoglou 2014; Lanas and Alvarez-Galindo 2003). Differently from cement mortars, in lime mortars, porosity increases by increasing the  $b/a$  ratio up to 2:1, increasing strength. Richer mortars show higher porosity because lime is a very porous material, and porosity allows faster and more complete carbonation (Lanas and Alvarez-Galindo 2003; Lanas et al. 2004). So, porosity reduces during curing since voids are progressively occupied by growing calcite crystals (Lanas and Alvarez-Galindo 2003; Lanas et al. 2004).

Considering the numerous factors affecting mortar and their variability, it is only through correct characterization of the historical mortar that it is possible to design new repair mortars. In (Veiga, José Aguiar, and Carvalho 2001), minimal requirements for rendering and repointing repair mortars are collected, considering the specificity of Portuguese construction and the results of many tests. The RILEM report (Groot et al. 2022), reviews theoretical backgrounds and laboratory research on the durability of lime-based mortars in conservation actions, including outcomes for pure air lime, lime-pozzolan, ternary binding systems (lime, pozzolan and cement), and data on long-term strength and porosity of repair mortars with different compositions. Discussions on characterization and development of suitable historic repair mortars are found in (Loke, Kumar, and Cultrone 2023); physical and mechanical performance criteria for new pointing mortars on historic structures are also reported in (Fontaine, Thomson, and Suter 1999; Peroni et al. 1981).

In (Veiga et al. 2008), the results of a large experimental investigation on lime mortars varying the composition is reported with the aim of carrying out a feasibility analysis. In (Philokyprou, Ioannou, and Ilia 2010), the results of an extensive investigation on crushed brick/lime mortars samples collected from various archaeological sites and historic buildings in Cyprus are presented and used to design and reproduce a series of compatible repair crushed brick/lime mortars. A series of characterization tests was also performed on such repair mortars. The research reported in (Papayianni et al. 2019) is based on the case study of the Galerius Palace in Thessaloniki, carried out from 1994 to 2006. The restoration operation concerned including the removal of eroded mortars and their replacement with compatible mortars. A significant number of compatible repair mortars were used, based

on the systematic study and analysis of existing ones. The repair mortars used were analysed 20 years later. Kumar and Kumar (2022) present the results of an extensive investigation conducted on lime mortar samples from ancient Indian temples, UNESCO sites, and on selected repair mortars with the addition of pozzolana.

According to the state-of-the-art and ICOMOS principles, it is crucial that the design of compatible repair mortars is based on efficient protocols and deep knowledge of the original material characteristics. Many researchers have delved into the methods for characterizing historical mortars combining consolidated standard methodologies with innovative procedures. In particular, the observation of thin sections under a polarized light optical microscope is the fundamental test in the process of characterizing a historical mortar, providing a large amount of information about the texture, microstructure, the kind of binder and the aggregate composition (Aggelakopoulou, Ksinopoulou, and Eleftheriou 2022; Borsoi et al. 2019; Bunaciu, Udriștioiu, and Aboul-Enein 2015; Columbu, Sitzia, and Verdiani 2015; Diamond 2004; Drougkas et al. 2023; Kaklis et al. 2018; Mechling and Baquet 2022; Pecchioni et al. 2008; Riccardi et al. 2007; Silva et al. 2010; Soares et al. 2023). Despite numerous studies on the methodologies for analyzing historical mortars and the specifications for compatible repair mortars for conservation actions, the gap between scientific knowledge and application needs for the mix design of compatible mortars has not yet been filled.

The study reported here aims to improve the usefulness of mortar characterization tests and provide quantitative indicators and acceptance criteria for defining repair mortars as compatible. To these aims, the paper primarily reviews the mortar characterization tests and how these parameters can help in the quantitative definition of compatibility criteria. Then, a two-part procedure, consisting of (i) characterization tests implementation, including Digital Image Analysis of the thin sections, and (iii) preparation, testing, and, eventually, correction of the new admixture, is proposed. Finally, the proposed methodology is applied and validated to the case study of the Casemates complex in Algiers.

## 2. Characterization tests on historic mortars for new mix design

Different techniques are employed to characterize historical mortars, depending on the type of information to extrapolate and the quantity of material available. The selection of the tests is severely conditioned by the size

and shape of the samples that can be extracted on site, which are of the order of just a few centimeters and show irregularities since material availability is often limited by the need not to damage the construction. Nonetheless, given the heterogeneity of historical materials, the characterization process should ensure statistically significant sampling. The extraction location and the number of samples should be appropriately evaluated. Moreover, the investigations mentioned in the following paragraphs are those considered as necessary for the procedure proposed in the present study and are not exhaustive of all the possible ones to be carried out on historical mortars. In particular, the procedures included are considered a subset essential to implement an actionable procedure for the mixed design of repair mortars and to allow the definition of quantitative criteria for validating the compatibility of the designed mortars with the original one. In the following, these investigations are presented in the order in which they are appropriate to be carried out in the proposed procedure.

The mechanical characterization of a historical mortar can only be obtained with indirect methods, as it is impossible to extract proper samples to be subject to mechanical tests. The drilling PNT-G technique is a non-destructive in situ test that allows the estimation of the compressive strength of the mortar joint, characterized by low compressive strength (as usually in the masonry walls of historical buildings). The PNT-G penetrometer equipment is composed of an ordinary battery hand drill able to generate a small cavity of 5 mm in depth so as not to cause damage to the mortar. An electronic control device measures the energy amount spent in the drilling and calibration curves allow a correlation between energy spent and mortar compressive strength. The drilling test is easy to carry out, non-destructive and validation tests have demonstrated its effectiveness in estimating the compressive strength (Carpinteri, Dimastrogiovanni, and Pugno 2004; Costa, Magalhães, and Do Rosário Veiga 2012; Gucci and Barsotti 1995).

Many studies on the mechanical properties of brittle materials such as concrete, mortars, and masonry have highlighted a link between compressive strength and elastic modulus. For concrete national and international design codes (Noguchi et al. 2009), provide several simplified formulas, based on many experimental data (2021). It is also important to underline that, for mortar, the modulus of elasticity depends very much on the properties of the aggregate, while the compressive strength depends mainly on the properties of the (Benedetti and Tarozzi 2020; Feo et al. 2016).

Concerning mineralogical tests, the diffractometric analysis carried out on a sample of mortar reduced to powder allows the determination of the global mineralogical composition without distinction between binder and aggregate. The diffractometric analysis is a qualitative and semi-quantitative analysis that uses X-rays to determine the crystalline structure, grain size, deformation, and defects of the crystals (Ali, Chiang, and Santos 2022). Given the small dimensions of the sample for the diffractometric analysis, the test is practically non-destructive. The powder of the sample, hit by radiation with a known monochromatic wavelength, diffracts this radiation at a certain angle, which depends on the distance between the planes of the crystal, a specific characteristic of each crystalline phase present in the sample. In addition to the overall mineralogical composition, diffractometry analysis allows us to highlight, through the presence of certain mineralogical phases, the phenomenology of degradation in progress or that has already occurred, characteristic of a particular type of lime; for example, the presence of hydromagnesite suggests that magnesium lime has been used and larnite suggests that the binder is hydraulic (Arizzi and Cultrone 2021).

As regards the physical parameters, bulk density, and porosity are considered for their link with mechanical properties and durability (Barsottelli et al. 1998; Cnudde et al. 2008; Karagiannis et al. 2016; Lanzón and García-Ruiz 2009; Veiga, Magalhães, and Bokan-Bosilikov 2004). Bulk density is defined as the ratio of the mass of a solid and the apparent volume (or geometrical volume). There are two direct methods for determining bulk density: the hydrostatic balance and the mercury pycnometer, both included in (ISO20290–1 2021). These methods are particularly desirable for irregularly shaped samples such as mortar extracted from masonry. The bulk density is a measure of the compactness of the material, which is related to its mechanical properties. The water-accessible porosity (or effective porosity) consists of pores where water can enter. This parameter can be measured through the hydrostatic balance method and mercury pycnometer. The water-accessible porosity indicates degradation vulnerability due to water infiltration, which can penetrate the accessible pores of mortars exposed to external environments. Mortars that have absorbed water can suffer a general loss of coherence, with possible disintegration and pulverization due to the freezing or crystallization of the salts.

The thermal expansion coefficient (TEC) is one of the most important thermo-mechanical properties of

mortars because temperature changes cause a pronounced alteration (Kwame 2008; Sicat et al. 2013; Siegesmund, Sousa, and Knell 2018; Zeng et al. 2012). Thermal deformation is significantly influenced by porosity, moisture, mineral composition, and texture of the mortar (Kwame 2008; Siegesmund, Sousa, and Knell 2018; Zeng et al. 2012). The pore water is proven to have a significant influence on the material TEC because liquid water has a larger TEC than the solid skeleton of material, and the pore water can accumulate stress during the thermal process (Ghabezloo 2011; Hover 2011). Two methods are suggested in (EN1770 2000) to determine TEC in inorganic repair mortars. TEC is not easily achievable on historical mortar samples, while specimens can be easily determined on repair mortar samples. Also, thermal conductivity tests (ISO113578 2021) are hardly applicable to historical mortar specimens due to the difficulties of extracting regularly shaped and equal specimens.

Concerning petrographic tests, the observation of thin sections under the microscope in transmitted polarised light is the most significant test for the characterization of a historical mortar; some images of thin sections analyzed by the authors are shown in Figure 1. The optical microscope's observation technique provides a large amount of qualitative information about the principal textural characteristics and compositional features of materials, such as macroporosity and distribution and shape of the surface pores (Figure 1(a-e)), possible additives, hydraulic products, residues from binder firing processes (Figure 1(f-g)), binder recrystallisation phenomena (Figure 1(h)), reaction rims around the aggregates (Figure 1(i)); or fragments of cocciopesto (Figure 1(l)) can be also identified through thin-section analysis and related to manufacturing technology and location of material extraction. Shrinkage cracks can also be detected (Figure 1(d-e)).

Digital Image Analysis (DIA) applied to thin sections of materials observed under the microscope has boosted the effectiveness and rapidity of characterization procedures. DIA, through the software ImageJ (<https://imagej.net/ij/download.html>), has proven to be a flexible and accurate analytical tool for inspecting the morphological or compositional characteristics of an image, capable of identifying qualitative and quantitative descriptors such as the number of objects, percentage of occupied areas, classification of color intensity or brightness. Complex combinations of descriptors such as roundness, shape factors, relative distance as a function of size, correlation criteria based on position and shape, etc., can be easily detected and quantified as

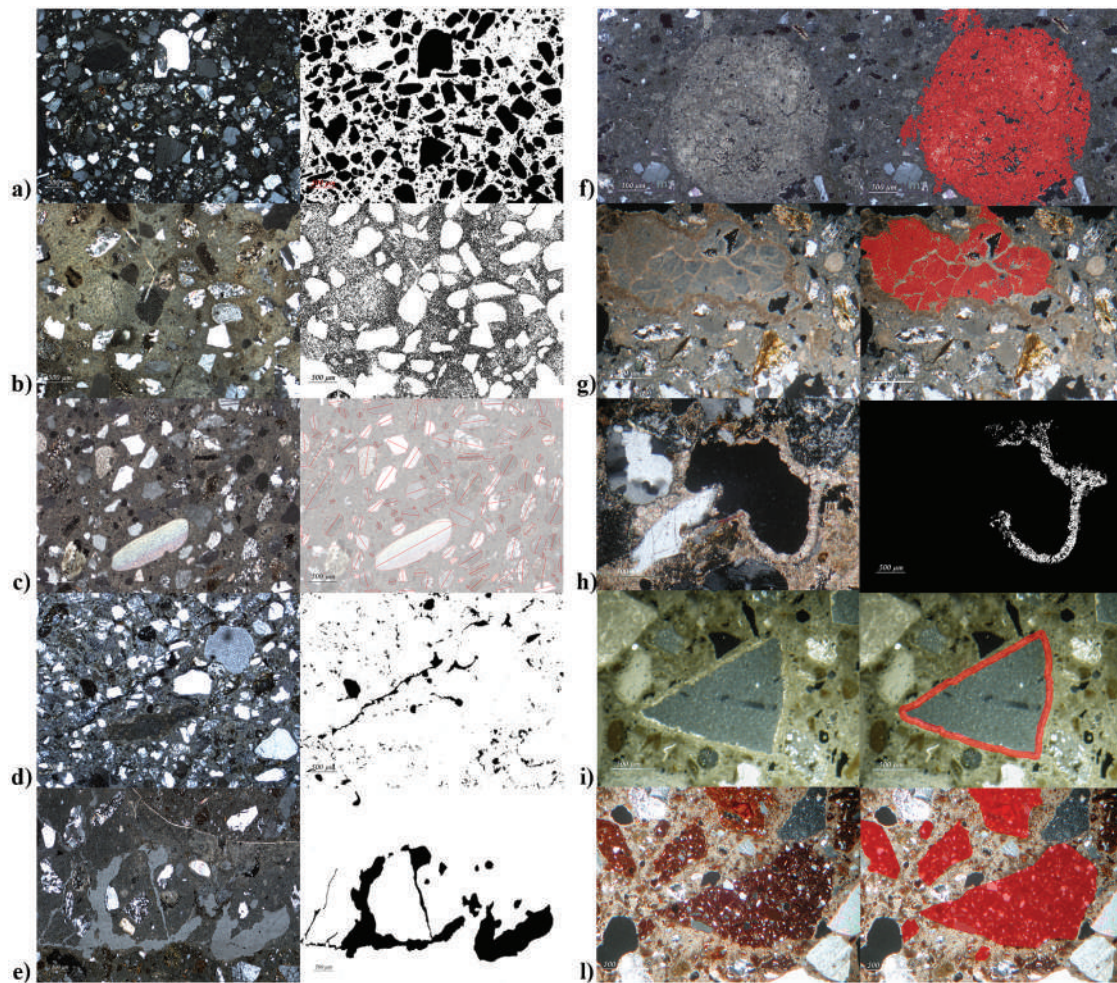


**Figure 1.** Thin section of bedding mortar and corresponding elaboration from: a) Tornabuoni chapel in Santa Maria Novella, Florence (15th cent.): a good granulometric classification of the aggregate; b) Brunelleschi's Dome, of the cathedral of Santa Maria del fiore, Florence (15th cent.): abundant binder without shrinkage cracks; c) rocca della Gorgona (13th cent.): orientation of the aggregate granules; d) Palazzo Davanzati, Florence (14th cent.): shrinkage cracks "closed" following chemical reaction processes; e) Casemates of Algeria (16th cent.): large amount of porosity; f) Fortress of San Rocco -Grosseto (18th cent.): lump of binder; g) Pietrasanta's Dome (16th cent.): "marble" of a stone of "travertine" ; h) Fortress of Verruca -Pisa (13th cent.): reprecipitation of calcite is observed near the porosity holes; i) Archaeological site of Foligno (1st cent. B.C.): "reaction edges" around flint fragment; l) Terme di Fiesole (1st cent. B.C.): cocchiopesto fragments. The analysis is carried out through the optical microscope in transmitted polarised light with parallel Nicols and crossed Nicols, with objective magnifications from 2.5X to 40X, on sample sections brought to a thickness of 0.03 mm to become transparent to light glued into special slides.

well (Levaldi and Fabbri 1986; Mendoza and Lu 2015). DIA applied to images of thin sections observed under an optical microscope has been exploited to determine the surface porosity of mortars and concretes (Chong et al. 2021; Reedy 2006), the granulometric curves of aggregates of mortars and concretes (Marinoni et al. 2005; Reedy 2006; Sitzia, Beltrame, and Mirão 2022), the sand grain roundness and other morphological characteristics of the aggregates (Sitzia, Beltrame, and Mirão 2022), and the ratio between binder/aggregate (Blauer and Kueng 2007; Carò and Di Giulio 2004; Marinoni et al. 2005; Piovesan, Mazzoli, and Maritan=2023).

### 3. Compatibility criteria

As well known, the use of inappropriate materials in conservation actions can produce many damaging effects as often observed in restored buildings (Apostolopoulou et al. 2018; Groot et al. 2022; Szemerey-Kiss and Török 2017). Consequently, the use of compatible materials is promoted in the principles enshrined in the ICOMOS charters on conservation and structural restoration of architectural heritage (Dimitrova et al. 2020; ICOMOS 2003, 2001; Roca 2011) which aims to avoid undesirable side-effects, including assessments of long-term impacts. In many

studies and Technical Committees reports (Do Rosario Veiga et al. 2010; Fontaine, Thomson, and Suter 1999; Groot et al. 2022; Loureiro et al. 2020; Nogueira, Paula Ferreira Pinto, and Gomes 2018; 2012; Roca 2011), compatibility between historical and repair mortars includes chemical, physical, and mechanical aspects, along with aesthetic appearance issues (color and superficial texture).

According to (Rodrigues and Grossi 2007), the concept of compatibility is complex and nuanced and cannot be reduced to a simple yes or no answer. Instead, it shall be considered from a broader perspective that includes environmental and sociological aspects as well as physical and chemical performances. Indeed, compatibility cannot be judged in absolute terms and must be analyzed in the context of each specific intervention, including the materials, the site, and the surrounding conditions. According to the cited study, a method for evaluating the compatibility of conservation actions through measurable indicators (physical, environmental, socio-cultural) shall be fostered. These indicators (e.g., the type of binder, additives and additions, type, form, and dimensions of aggregates, porosity, water vapor permeability, strength, and deformability, etc.) are integrated into a uniform rating system, within which each indicator can range from 0 to 10. The lower the rank, the closer the physical/mechanical parameter values of the original and the repair mortars

In the present work, and in accordance with the previously cited studies, the technical characteristics for compatibility between historical and new mortars considered are:

- chemical composition (binder, aggregate type, and binder/aggregate ratio) and aggregate particle size distribution.
- mechanical strength
- open porosity
- thermal expansion coefficient

Similar composition guarantees, first of all, homogeneity in the physical and mechanical behavior of the two materials in contact. If there is much difference in stiffness between the new mortar and the historical one, shear stress at the interface between the two materials increases, causing the detachment or, in any case, the lack of structural collaboration (Bocca and Grazzini 2012, 2013). To avoid damage to the historical mortar, the repair mortar should have lower mechanical characteristics than the historic one.

The porosity properties of a mortar are closely linked to its mechanical properties and vulnerability to degradation due to water infiltration. The porosity depends on the composition of the mortar, as a greater quantity of water produces higher porosity. Assuming that the repair mortars must not degrade the mortar on which it is applied, the porosity of the repair mortar should be higher than the historical one so that the water vapor is mainly absorbed by the repair mortar to collect soluble salts (Apostolopoulou et al. 2018; Klug et al. 1969; Rodrigues and Grossi 2007).

The difference between TEC of contacting materials subjected to thermal variations produces concentrations of interface shear stress due to the different thermal strains. This produces fractures and loss of cohesion. Acceptable TEC values of historical mortars are available in the literature (Černý et al. 2006; Van Balen et al. 2007).

The in-depth analysis of the literature on repair mortars has made it possible to identify the values for the technical characteristics of the repair lime mortar, Table 1. Validation criteria for the physical and mechanical properties of designed repair mortars have been defined based on the general compatibility criteria for conservation actions and literature data, Table 1. The proposed criteria are based on comparing experimental results obtained on the historical and new mortar. Considering the fundamental characterization tests that can be easily carried out on historical mortars, the validation criteria focus on compressive strength (to which the elastic modulus is linked) and open porosity (which is linked to the bulk density):

- compressive strength (evaluated through a penetrometer) of the repair mortar must be less or equal to that historical;
- repair mortar's open porosity evaluated through the hydrostatic balance (ISO20290-1 2021), must be greater or equal to the historical one.

In agreement with Rodrigues and Grossi (2007) for both criteria, a 20% difference between the values of the repair mortar compared to the historical mortar can be considered acceptable as a validation criterion. The value of 20% was assumed, considering that in heterogeneous materials (such as historical ones), a 20% coefficient of variation in mechanical properties is deemed acceptable to the characterization value. If, in addition to strength and porosity, it is also possible to determine the Thermal Expansion Coefficient (TEC) of the repair mortar, the values obtained must be under the range value in the literature.

**Table 1.** Ranges for compressive strength,  $\sigma_c$ , Young's modulus,  $E$ , porosity,  $P$ , and bulk density,  $\gamma$ , according to (1) Veiga, José Aguiar, and Carvalho (2001); (2) Groot et al. (2022); (3) Loke, Kumar, and Cultrone (2023); (4) Veiga et al. (2008); (5) Philokyprou, Ioannou, and Ilia (2010); (6) Papayianni et al. (2019), (7) Kumar and Kumar (2022); Peroni et al. (1981), (8); Van Balen et al. (2005), (9); Černý et al. (2006), (10). Letters next to the reference key indicate different types of mortar reported in the cited study. Mortar type keys: a = air lime, H = hydraulic Lime; the column "add" shows the following keys for additives: C = cocciopesto, p = Pozzolana; \*dynamic modulus.

#	type	add	$\sigma_c$ [MPa]	$E$ [GPa]	$P$ [%]	$\gamma$ [g/cm <sup>3</sup> ]	TEC x10 <sup>-6</sup> (°C <sup>-1</sup> )
4c	A	C	0.70–1.00	4.35			
5a	A	C			30–52	1.10–1.80	
5c	A	C	2.16–3.97	0.42*-0.55*			
6a	A	C	2.50–4.00		29–38	1.20–1.50	
6b	A	C	1.00–5.00		15–38		
8c	A	C	0.70–0.80	1.44–1.60	35–37	1.88–1.92	
10b	A	P	0.44–4.06		32–45		6–15
2b	A	P	2.50–4.50		26–30	1.57–1.80	
4d	A	P	0.50–0.90	2.49–3.92			
6b	A	P	2.01–5.40		26–35	1.57–1.80	
7b	A	P	0.39–0.90			2.18–2.24	
8b	A	P	0.62–0.92	0.75–1.33	29–31	1.91–1.95	
10a	A		0.97–1.11		34		12
1a	A		0.60–3.00	3.00–6.00			
4b	A		0.60–1.60	2.3–4.1			
5b	A		0.94–2.57	0.2–0.52*			
7a	A				41–55	1.03–1.14	
9a	A						3–7
8a	A		0.59–0.91	0.75–5.56	25	1.9–2.14	
4a	A+H		0.60–1.00	1.64–1.85			
3	H		1.00–8.00	1.00–8.00	20		
4e	H		0.60–3.10	1.13–7.51			

## 4. The proposed methodology

### 4.1. The two-part procedure

The procedure proposed for designing a new repair mortar with compatible characteristics compared to a historical mortar comprises two parts, and the flow chart is reported in Figure 2. The first part comprises the collection of a series of data obtained through in-situ and laboratory analyses on the original mortar, and the main steps include:

- In situ penetrometric investigations, to estimate the compressive strength ( $\sigma_h$ );
- Sampling of historical mortar, balancing difficulties in extracting quantities of material and needs for representativeness and statistical value;
- Laboratory investigations on the samples taken for the determination of the basic physical parameters: bulk density ( $BD_h$ ) and water-accessible porosity ( $P_h$ );
- Diffractometric analysis on the samples taken;
- Petrographic analysis via observation on thin sections of samples taken under the microscope in transmitted polarised light;
- Digital Image analysis (DIA) of the thin sections observed under the microscope (subsection 4.2 is dedicated to a detailed description of this fundamental step);
- Definition of the mix design in terms of binder/aggregate ratio, type of binder, type and grain size of the aggregate and water amount;
- Production of samples of new mortar based on the mix design;
- Penetrometric investigations on samples of new mortar for the estimation of the compressive strength ( $\sigma_r$ ), to perform a direct comparison with the corresponding data obtained on historical mortar; the age of samples should be greater than 60 days;
- Physical tests on samples of the new mortar for the determination of bulk density ( $BD_r$ ) and water-accessible porosity ( $P_r$ ) to compare the value with the historical ones;
- Test for the determination of thermal expansion coefficient ( $TEC_r$ ) on samples to compare the value with the literature range value:  $3 \times 10^{-6} \text{ C}^{-1} \leq TEC_r \leq 15 \times 10^{-6} \text{ C}^{-1}$

The second part of the procedure consists of defining the mix design based on the data collected and the manufacturing of the new mortar samples. Characterization tests are carried out on these samples to obtain experimental data comparable to the historical mortar. To validate the mix design, compatibility criteria must be employed. If the new mortar does not pass the validation test, changes to the mix design are defined through an iterative logic. The steps of the second part of the procedure are:

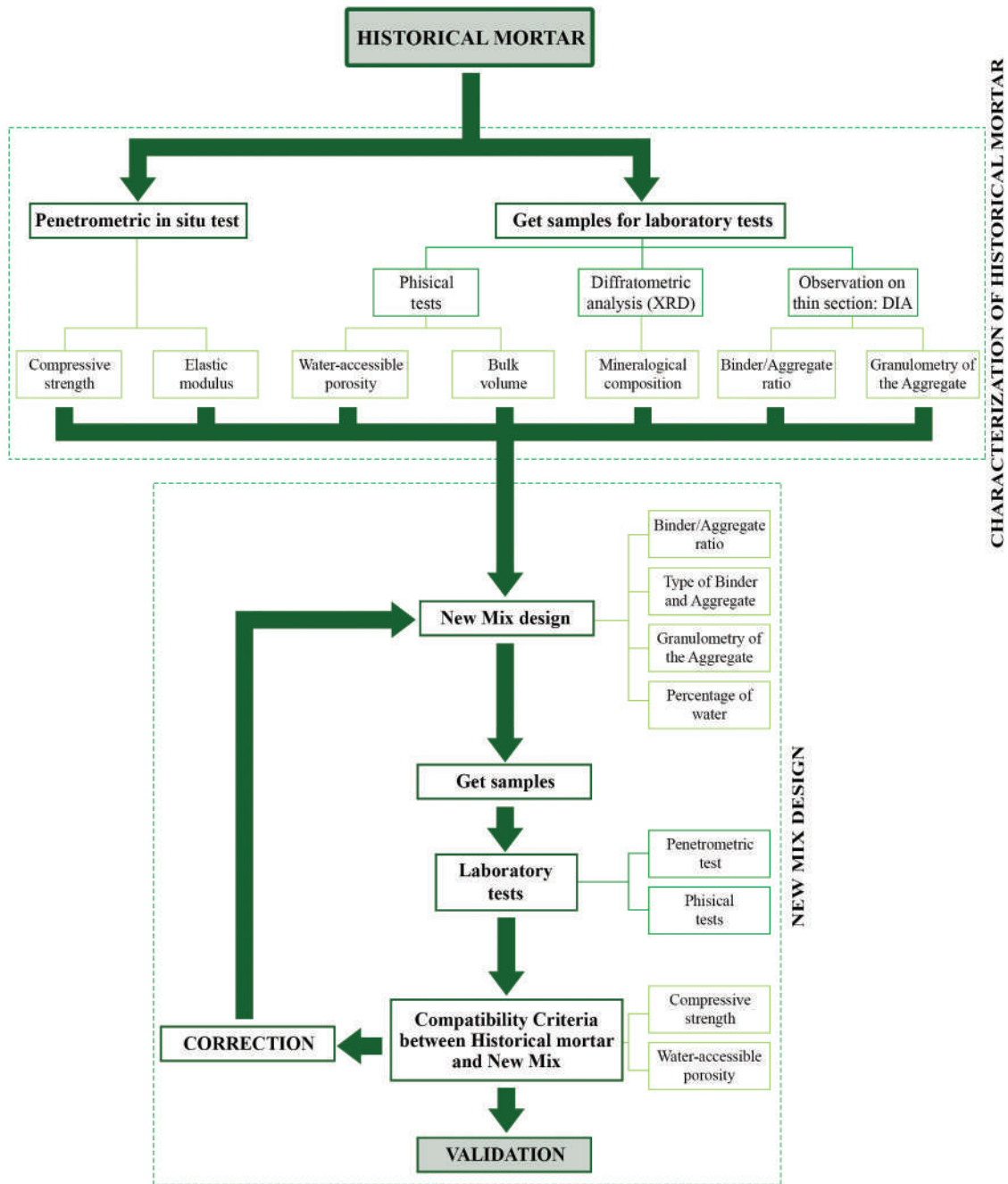


Figure 2. Flow chart summarizing the main steps of the proposed procedure.

- Application of compatibility criteria to validate the mix design based on the experimental data through a direct comparison between historical and new mortar data for compressive strength and water-accessible porosity.

$$\begin{aligned} (\sigma_h - 0.2\sigma_h) &\leq \sigma_r \leq \sigma_h \\ P_h &\leq P_r \leq (P_h + 0.2P_h) \end{aligned}$$

with  $P_r$  and  $P_h$  the porosity of the repair and the historical mortar, respectively, and with  $\sigma_r$  and  $\sigma_h$ ,

the compressive strength of the repair and historical mortar, respectively.

- correction of the mix design
  - if the repair mortar meets both criteria, the mix is accepted;
  - if the repair mortar does not satisfy one or both criteria, the mix must be adjusted through small steps of variation in composition. For the mix variations, it shall be recalled that (1) increasing the b/a ratio increases strength and stiffness; (2)

for a fixed ratio  $b/a$ , increasing the percentage of water decreases strength and stiffness and increases the open porosity.

It must also be highlighted that the stated mechanical compatibility criterion explicitly addresses compressive strength only because determining the elastic modulus for mortar alone in situ is impossible. However, it is known that correlation expressions are available in the literature that can provide an estimate of the elastic modulus as a function of the strength, Marastoni et al. (2017). The physical compatibility criterion explicitly includes water-accessible porosity only, although, in this case, an inverse correlation exists between porosity and bulk density. Hence, by validating porosity, density is also taken into account.

It is worth underlining that a complete characterization of the repair mortar includes, in addition to indirect tests, such as the penetrometer test, also direct mechanical tests, such as the three-point bending and the compression tests on the resulting prism halves, and the compression on prisms for the modulus of elasticity.

#### 4.2. Image analysis of the thin section of historic mortar

The core of the procedure consists of analyzing the image of the thin section of the historical mortar. The thin section shall be examined and photographed using a transmitted light microscope with both crossed and parallel Nicols frames; a photo merge might be necessary to reassemble the complete image of the thin section. Then, it is necessary to establish the dimensional scale, with appropriate conversion from pixels to lengths. The scaled image is converted into an 8-bit greyscale using image processing software. Then, the segmentation phase can begin. In this study, the software used for image segmentation and quantitative analysis was ImageJ (<https://imagej.net/ij/download.html>) because it has been widely employed for similar purposes, as already reported in the previous sections. Segmentation consists of isolating only the areas in the image containing the desired information (generally lines, curves, and areas) by picking pixels with similar gray levels within specified thresholds through the dedicated command; manual finetuning of the automatic color picking might be necessary.

A clear distinction between binder and aggregate is possible through segmentation, and subsequent analyses to detect aggregate total area, grain size, shape, and distribution within the binder can be implemented (Figure 1(a-c)).

The particle analysis phase counts and measures objects, i.e., clusters of black pixels, named Region of Interest, ROI. The analysis outlines the object by approximating the shape through a best-fit ellipse; minimum size and circularity thresholds can be adjusted. For each ROI, area, Feret diameter, and minimum Feret diameter (Figure 1(c)) are tabulated. The Feret diameter is the longest distance between any two points along the ROI boundary, and it is also known as the maximum caliper length; while the minimum Feret diameter is the minimum caliper length. Both measurements are useful for defining the granulometric distribution. For each grain, i.e. a detected object, the  $\tilde{\phi}$  parameter is calculated as  $\tilde{\phi} = -\log_2 d$ , where  $d$  is the minimum Feret diameter; in this way, a class of the grain can be attributed and granulometric distribution obtained (Carò and Di Giulio 2004).

The Feret angle can also be extracted in particle analysis and can provide indications regarding the orientation of aggregates, Figure 1(c).

Concerning porosity that can be estimated through DIA, it shall be underlined that this measurement clearly refers just to the voids detectable on the planar surface of the thin section and cannot be directly related to the water-accessible porosity (referred to the specimen volume) determined through dedicated tests (see section 2). Nevertheless, surface pore distribution can provide still useful information when comparing the original mortar with a newly designed mix. Both cross and parallel Nicols images must be utilized to extrapolate the area affected by the pores. The two RGB images are overlaid with a 50% opacity level with the aim of identifying the gray level typical of the filler resin common to both images. Subsequently, the overlaid image is converted to 8-bit grayscale. The gray of the filler resin due to the cavities and microfractures is visually detected and automatically picked over all the images through appropriate threshold definition. In so doing, a binarised image made of black objects can be quantitatively analyzed and extracted, Figure 1(d,e). Once aggregate and porosity areas have been evaluated, the area occupied by the binder can be extracted by subtraction.

## 5. The case study of casemates of algiers

### 5.1. Description of the complex and its pathologies

The Casemates building, an Ottoman military structure, is part of the Citadel, which dominates the heights of the Kasbah of Algiers. The construction of the Citadel began under the direction of Sultan Aroudj Barbe

Erousse and was completed in 1592 under the governance of Kheder Pacha (Buresi et al. 2018; Gaid 1974). For its historical, cultural, and architectural value, the Kasbah of Algiers, including the Citadel, has been inscribed on the UNESCO World Heritage list since 1992. The Casemates building, integrated into the rampart of the Citadel, was designed to shelter soldiers, weapons, and provisions, enabling solid protection during conflicts. The Casemates building represents an exceptional example of Ottoman military engineering for the employed construction techniques, architectural features, and integration into the Citadel. The complex comprises the union of two parallelepipeds, slightly misaligned contiguous blocks, resulting in a very long (28 m) and narrow (8.5 m) building. Each block is organized into three levels: the ground floor and the first-floor house magnificent galleries, characterized by a long sequence of cross vaults; the last level consists of the terrace adorned with loopholes (Abderrahim Mahindad 2017). In (Figure 3(a,e)), general views, a plan, and a cross-section of the building are reported.

The external walls facing northeast coincide with the fortified walls of the Citadel. They are, therefore,

very thick, 1.4 m, and consist of a rubble wall made of two external brick facings and an internal filling core (Abderrahim Mahindad 2017), (Figure 3(b)) and (Figure 4(c)). The other external walls of much smaller thickness and internal separation walls are made mainly of brick but also of mixed brick and stone (Abderrahim Mahindad 2017), (Figure 4(a,b)). Over time, the Casemates building has suffered various structural damages and currently, the repair interventions foreseen by a conservation project started in 2005 have not yet been completed. The building is affected by a significant fracture pattern that crosses the vaulted galleries longitudinally on both floors and by various minor fracture patterns and damage to the masonry.

Several other types of degradation also affect the complex. The mortars, employed both for bedding and plastering, represent a relevant vulnerability of the building because its deterioration and loss of homogeneity and continuity severely threaten the integrity of the masonry. The source of these degradations is chemical in nature and primarily results from humidity and ambient pollution. Alkaline lime

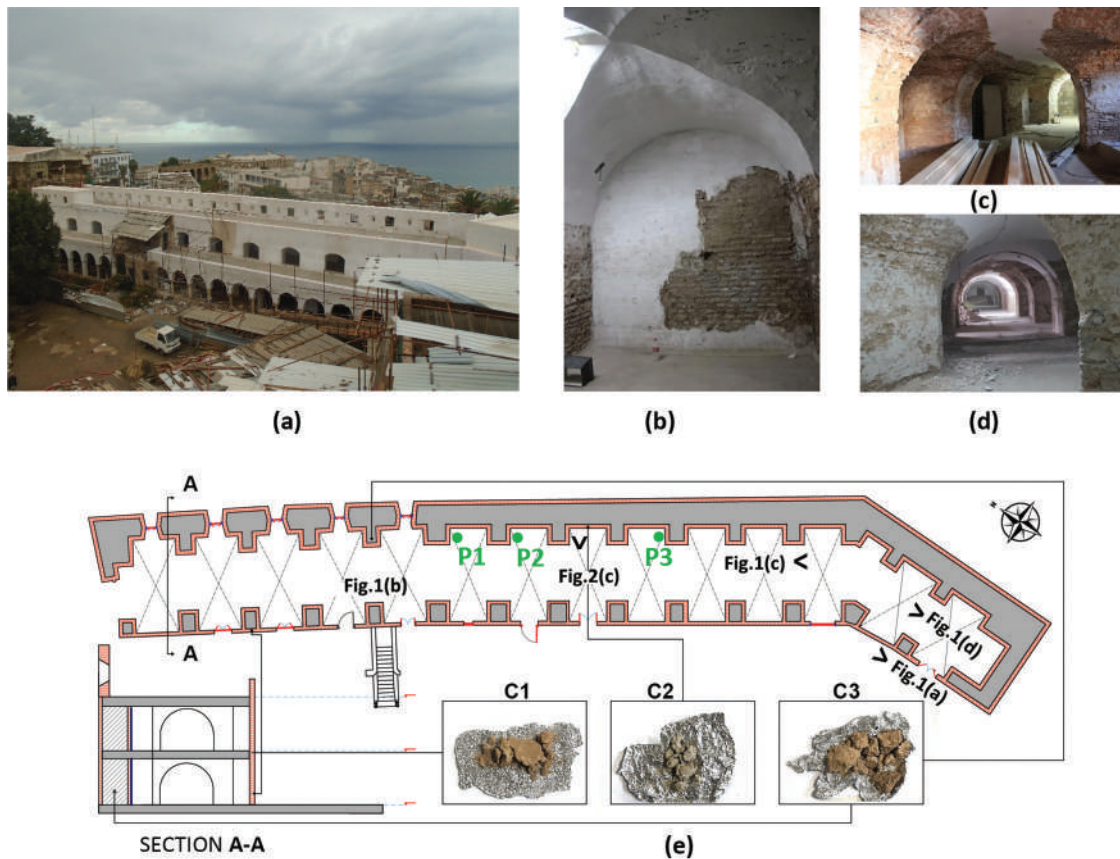


**Figure 3.** The casemates building in the citadel of the Kasbah of Algiers: (a) external view; (b-d) internal views; (e) plan and section with localization of photographs (c-d) and extraction of mortar samples and areas subject to penetrometer tests.

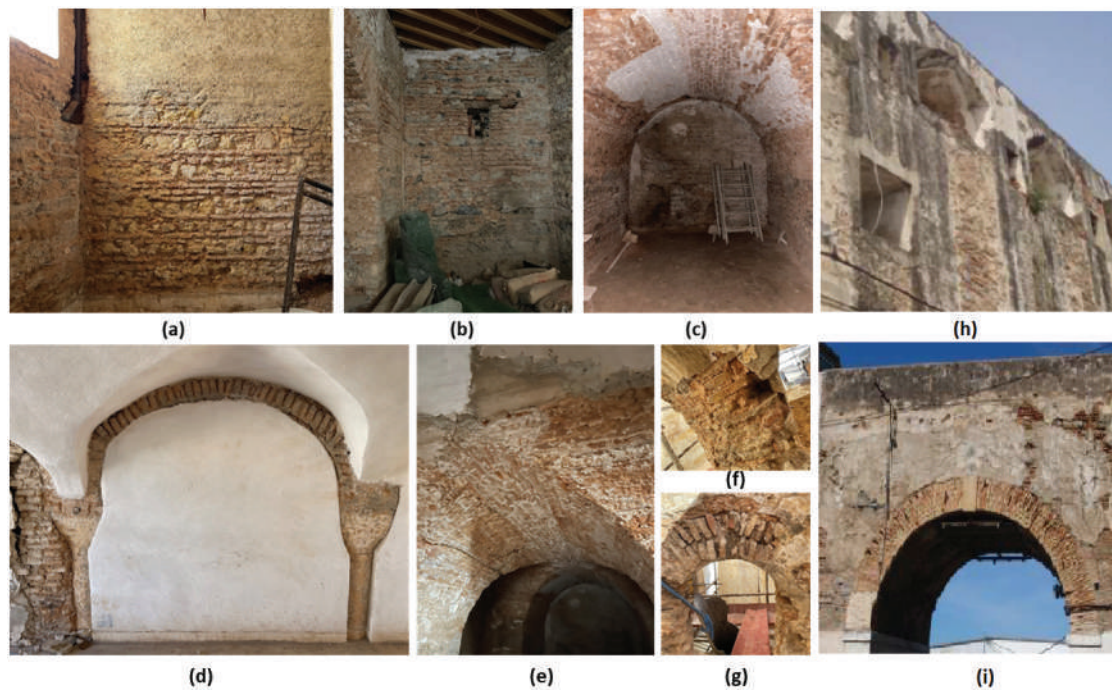


**Figure 4.** The casematte building: (a-c) examples of wall textures; (d-g) examples of damage requiring repair mortar; (h-i) examples of pathologies extracted from the work of N. Mahindad.Abderrahim Mahindad (2017).

mortar is particularly sensitive to the action of acids present in the air or water. This phenomenon leads to a series of chemical reactions that generate salts like sulfates and crystallize within the masonry (Van Hees et al. 2004)., This chemical alteration has led to a significant loss of material, manifesting in visible phenomena such as flaking, peeling, crumbling, swelling, and detachment, especially in the north-east at the level of the roof terrace. Furthermore, biological alterations have also been observed. The colonization of mortars and plasters by algae, moss, and lichens develops under the combined effect of humidity, heat, and light. Mosses are particularly present on the northeast side, which is facing the sea, favoring persistent humidity conditions. On the other hand, Lichens mainly feed on limestone and can penetrate deeply into the support, thus aggravating existing damage. Figure 4(h) illustrates cases of detachment and cracking of the plaster linked to this biological colonization, and Figure 4(i) also shows deposits of black encrustation on the façades. Additionally, water stagnation, particularly on horizontal surfaces, leads to the deposition of calcite on the surface of the materials. These deposits generate salt crystals and the appearance of white encrustations or efflorescence, as shown in Figure 4(i).

The procedure proposed in this article was applied to the design of a repair mortar compatible with the original one for the filling of joints and the repair of damaged

wall portions in cases similar to those represented in Figure 4(d-g).

## 5.2. Materials and methods

To characterize the mortars of Casemates, a series of site and laboratory analyses were implemented. Site tests consisted of the penetrometer test carried out on the mortar joints in three locations:

- P<sub>1</sub> refers to the bedding mortar of the north internal wall of the 6th groin vault at the first level of the complex, the joint was sampled from an area partially undisturbed from degradation phenomena at an height of 0.8 m;
- P<sub>2</sub> refers to the bedding mortar of the north internal wall of the 7th groin vault at the first level of the complex, the joint was sampled from an area partially undisturbed from degradation phenomena at an height of 1.5 m;
- P<sub>3</sub> refers to the bedding mortar of the north internal wall of the 9th groin vault at the first level of the complex, the joint was sampled from an area partially undisturbed from degradation phenomena at an height of 1 m.

Locations of the penetrometer test were close to points where the mortar was sampled for laboratory analyses and appropriately selected for representativeness

(Figure 3(e)), belonging to the most widespread wall typology. The tests were conducted on an uncovered wall to get direct access to the mortar joint. According to (Gucci and Barsotti 1995) for each test location, the measurement is considered reliable if at least 5 values differ from the average value of the 15 caves performed by less than 25%.

To implement laboratory analyses, mortar was sampled in three locations according to Figure 3(e), the samples  $C_1$ ,  $C_2$ ,  $C_3$  were labeled, weighted and catalogued:

- $C_1$  is a mortar from a wall on the ground floor, the sample consists of two different sections distinguished by two different colors, suggesting two types of mortar. The first section is yellow-orange, and the second is beige-rosy. The mortar is friable by hand;
- $C_2$  is a mortar from a wall on the ground floor, is a beige-rosy mortar, friable by hand, with the presence of red and brown particles;
- $C_3$  is a mortar of pillar on the ground floor, has a yellow-orange color and a texture that appears compact, but is friable by hand, with red and brown particles present.

The sampling locations were chosen considering the restoration context of the complex, prioritizing areas that had not been restored to access the historic mortar while preserving the aesthetic and restoration work. Accessible points, such as certain parts of walls  $C_1$  and  $C_2$ , or a pillar  $C_3$  already damaged, were selected to avoid causing further damage to the building. The sampling was carried out manually using minimally destructive tools, allowing for the collection of small quantities of mortar required for the tests, while minimizing the impact on the integrity of the complex.

The listed tests were implemented on specimens representative of each mortar sample:

- water-accessible porosity test, through the hydrostatic balance method using a hydrostatic Mettler Toledo model AG<sub>2</sub>0<sub>4</sub> balance, with sensitivity 0.001 g according to Columbu et al. (2022) on specimens P- $C_1$ , P- $C_2$ , P- $C_3$ ;
- bulk density test through the hydrostatic balance method using a hydrostatic Mettler Toledo model AG204 balance, with sensitivity 0.001 g according to Columbu et al. (2022) on specimens BD- $C_1$ , BD- $C_2$ , BD- $C_3$ ;
- XRD test to determine the principal mineralogical composition through an X'Pert PRO diffractometer by PANalytical equipped with an

X'Celerator detector and HighScore software for the acquisition and the interpretation of data according to the following operative conditions: CuK  $\alpha_1 = 1.545 \text{ \AA}$  radiation, 40 KV, 30 mA,  $2\theta = 3-70^\circ$ , on specimens X- $C_1$ , X- $C_2$ , X- $C_3$ ;

- Thin section analysis through direct observation using an Axio Scope A1-Zeiss, transmitted light microscope at  $2.5\times$  magnification and digital image semi-automatic analysis on the TS- $C_1$  and TS- $C_3$  thin section from specimens  $C_1$  and  $C_3$ .
- Colored images with crossed and parallel Nicols frames were taken with pixel dimensions  $13,820 \times 6292$  and  $12,054 \times 9150$  for  $C_1$  and  $C_3$ , respectively, with a resolution of 150 DPI in TIFF format, and the photo merge was carried out using Microsoft's ICE-Image Composite Editor software. Through the software ImageJ (<https://imagej.net/ij/download.html>) a three-step segmentation was implemented to extrapolate from the crossed nicols image the aggregate analysis employing the threshold interval equal to (130–255); (0–80). Then, the two segmented 8-bit images were overlaid, flattened, and smoothed where the ROI was not sufficiently clear. Finally, the aggregate analysis was implemented, requiring no grain size limitation and a circularity limit equal to 0.003 to extract the minimum Feret diameters. Surface porosity and binder percentage have been defined consequently through threshold values complementary to those defined for aggregate detection. For a subportion of the thin section of the sample  $C_1$ , the detection of the cocciopesto was implemented with a similar procedure and employing threshold values equal to (20–40).

### 5.3. Results

Penetrometric analysis provided an estimate of the compressive strength  $\sigma_h = 5.2 \text{ MPa}$ , the mean value of the three considered in-situ samples, with CV = 16%. The data obtained highlights a high value for the compressive strength of a historic lime mortar and is indicative of accuracy in production.

Concerning results of porosity, as reported in Table 2, the specimen P- $C_2$  showed the highest value, 21% higher than the average, while the lowest value was recorded for the sample P- $C_1$ , which showed a value 39% lower than the highest. These results are coherent with bulk density results since the lowest value,  $1.21 \text{ g/cm}^3$ , –20.9% compared to the average value, is found for BD- $C_2$ , associated with the highest porosity specimen. Although the specimen BD- $C_1$  showed the highest bulk density, 52% higher than the lowest (BD- $C_2$ ), it also showed the lowest porosity.

**Table 2.** Results of physical tests on the historical mortar.

Water-accessible porosity [%]		Bulk density [g/cm <sup>3</sup> ]	
P-C <sub>1</sub>	25.1	BD-C <sub>1</sub>	1.84
P-C <sub>2</sub>	41.2	BD-C <sub>2</sub>	1.21
P-C <sub>3</sub>	36.2	BD-C <sub>3</sub>	1.55
Average	34.1	Average	1.53
CV.	0.24	CV	0.21

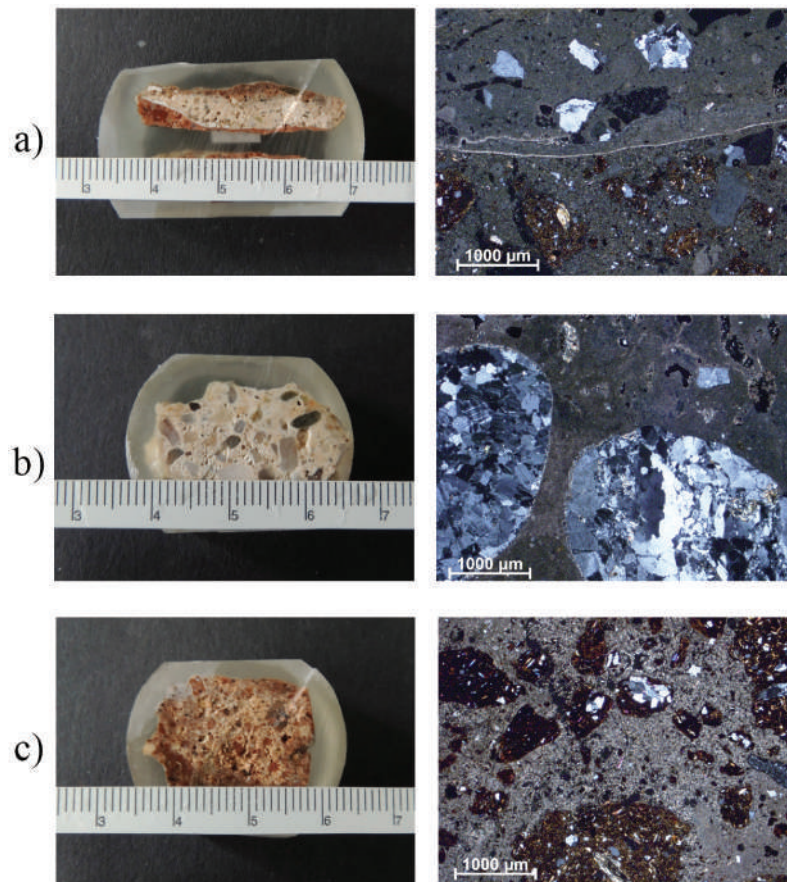
**Table 3.** Principal mineralogical composition (XRD) of three historical mortar samples.

	Calcite	Quartz	Feldspars	Micas
X-C <sub>1</sub>	xxx	xx	xx	x
X-C <sub>2</sub>	xxx	xx	xx	x
X-C <sub>3</sub>	xxx	x	tr	x

Concerning the mineralogical composition, the main phase common to all three samples is represented by calcite (Table 3). The presence of calcite refers to the carbonate binder, but traces of calcite could also be found within the aggregate. As for quartz, feldspars, and mica, they are silicates that indeed belong to the aggregate. For samples X-C<sub>1</sub> and X-C<sub>2</sub>, the same presence of quartz and feldspars is highlighted in

the second phase, while the presence of mica < 5%. For sample X-C<sub>3</sub>, it was recorded the presence of quartz and mica < 5%, trace feldspars (Table 3).

The petrographic study on thin sections shows different kinds of mortars. Sample TS-C<sub>1</sub> consists of two different portions, Figure 5(a). A mortar with a very abundant binder of pure air lime is present. The aggregate has an unimodal grain size of 400–600 μm and consists predominantly of sub-angular quartz grains and secondarily of carbonate fragments. In this mortar, the air lime was boosted in hydraulicity by adding “cocciopesto” (crushed bricks) with mixed granulometries. Quartz and mica granules with a size of 200–400 μm are also present. Lime lumps are absent in both mixtures. Sample TS-C<sub>2</sub> is an abundant binder mortar consisting of pure air lime. The aggregate shows an unimodal grain size of 1–1.5 mm, consisting mainly of polycrystalline quartz granules and rounded quartzites, Figure 5(b). Fragments of carbonate rocks are rare. Sample TS-C<sub>3</sub> consists of a very abundant binder of air lime, which was attempted to be made hydraulic by the addition of “cocciopesto” with much coarser granulometry, thus inhibiting the complete

**Figure 5.** Polished section and frame from thin section analysis in transmitted-light microscope with crossed nicols for specimens. (a) C<sub>1</sub>, (b) C<sub>2</sub> (c) C<sub>3</sub>.

formation of hydraulic compounds with lime, [Figure 5\(c\)](#). Rare carbonate fragments are also present. [Figure 6](#) shows the thin section TS-C<sub>3</sub>, where some cocciopesto grains are surrounded by darker halos, i.e., reaction rims due to hydraulic compounds.

The process of the Digital Image Analysis implemented on the historical mortar is described through the sequence of the extracted images reported in [Figure 7](#). From the DIA of the thin section image, it was possible to estimate the binder/aggregate ratio, the percentage of superficial porosity, and the grain size distribution. It is worth highlighting that a part of the aggregate is certainly not identified through this analysis. However, to carry out a test in which the binder is dissolved, the aggregate is recovered, and then the particle size distribution is assessed through sieving, would require a remarkable amount of material that might not be available. The DIA method is proposed as a simple and relatively quick

tool that can be applied even, admittedly with a margin of error, on small samples. Also, DIA can be applied in cases where carbonate aggregate is present. Moreover, if in the original mortar, cocciopesto had been added to promote a pozzolanic reaction with the formation of hydraulic compounds, calcium silicates, these could not be dissolved and would be added to the aggregate in the particle size distribution, altering the result.

For TS-C<sub>1</sub>, the b/a ratio of 1.6 was found through DIA. This ratio indicates a very rich mortar, with a significantly higher amount of binder than the aggregate. The percentage of superficial porosity found in the section is approximately 4%. For TS-C<sub>3</sub>, the b/a ratio 1.85 found indicates a greasy mortar characterized by abundant binder compatible with some shrinkage fractures highlighted by image processing. The porosity was found to be equal to 5%.

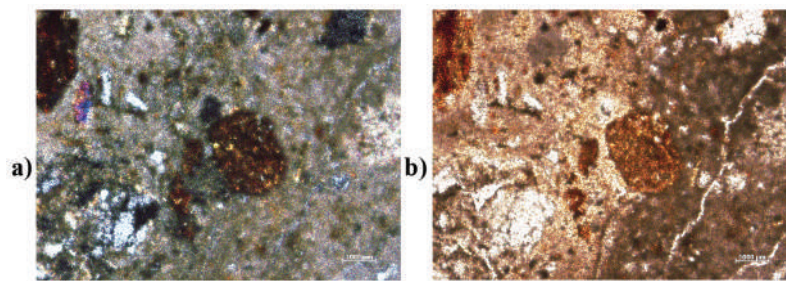


**Figure 6.** Zoomed 10 (10x) frame from thin section analysis in transmitted-light microscope with crossed nicols (a) and parallel nicols (b) for specimen TS-C<sub>3</sub> identifying the reaction rims of cocciopesto.

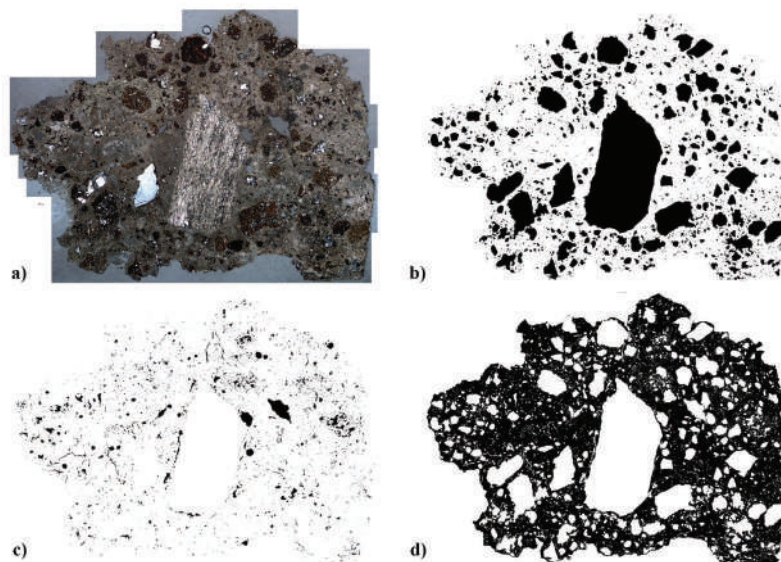


**Figure 7.** Digital image analysis: image segmentation process. (a) crossed Nicols image; (b) extrapolation of aggregate; (c) extrapolation of porosity; (d) extrapolation of binder.

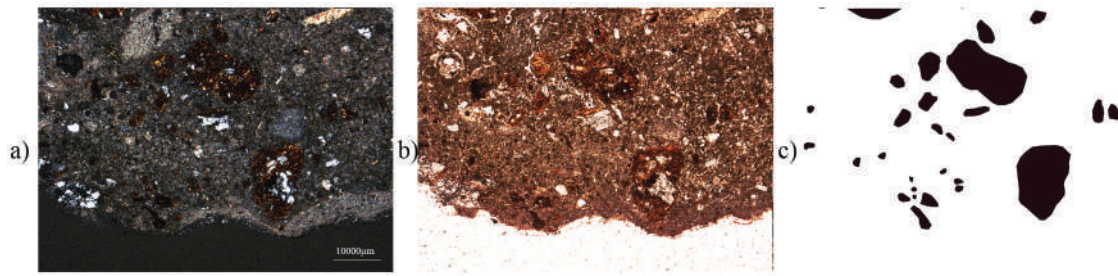


**Figure 8.** Zoomed 5 (5x) frame from thin section analysis in transmitted-light microscope with crossed Nicols (a) and parallel Nicols (b) for specimen TS-C<sub>1</sub> identifying the cocchiopesto through DIA (c).

To characterize the presence of cocchiopesto through DIA, a subportion of the thin section of TS-C<sub>1</sub> was considered, Figure 8. Manual segmentation was performed employing the already mentioned threshold values. The percentage of cocchiopesto found in the TS-C<sub>1</sub> was almost 10% of the considered surface, corresponding to approximately 38% of the aggregate. It should be highlighted that the larger cocchiopesto particles are easily detectable with the DIA while the smaller particles might be much more challenging. In our case, this may have led to the partial nondetection of cocchiopesto fine particles and so, the percentage obtained can be underestimated. Figure 10 and Table 5 show the results of granulometry analysis through DIA for TS-C<sub>1</sub> and TS-C<sub>2</sub>.

#### 5.4. Discussion

The petrographic study combined with mineralogical analysis shows that the analyzed samples have in common the high quantity of binder and the absence of lumps of lime, indicating care in the lime production process. Concerning the nature of aggregate, two different sources can be identified: a fine-grained sediment consisting of subangular quartz grains and a coarser sediment with rounded granules. In this case, the granules may derive from the disintegration of a quartz sandstone of aeolian origin or aeolian sands. Concerning mixtures containing cocchiopesto, the difference lies in the grinding accuracy, which makes the cocchiopesto more or less reactive and, thus, the mortar more or less hydraulic. An amount of cocchiopesto equal to 39% of the aggregate was detected, justifying the very red colour of the mortar.

The care in the lime production process highlighted by the petrographic analysis is further confirmed by the compressive strength value estimated through the penetrometric test. The value  $\sigma_h = 5.2$  MPa is, in fact, comparable to the maximum values of the compressive strength of lime mortars reported

as references for conservation actions in Table 1. In particular, the determined value is similar to that of the mortars reported in (Papayianni et al. 2019), the study labeled 6a in Table 1, which belonged to a monumental building in the Mediterranean area. Also, the corresponding value determined for the water-accessible porosity,  $P_h = 34.1\%$ , aligns with the results reported in (Papayianni et al. 2019), and provided in Table 1.

The grain size curves reconstructed through the DIA analysis for mortars C1 and C3 show a similar pattern, which is reasonable and expected given that these two mortars were made with the same sand and used simultaneously for the same purpose in the same building. It is, therefore, reasonable to assume that the sand comes from the same source.

## 6. Mix design and validation

### 6.1. Mix-1

Based on the analyses conducted on historical mortar samples, a mix formulation for a repair mortar, referred to as Mix-1, was developed, ensuring it was sufficiently close to the original to guarantee compatibility with existing materials, see Figure 9.

Concerning the choice of the binder, the potential application of the newly designed mixes was carefully considered. First, the new mix is not intended for plastering but for structural consolidation; hence, adequate performance in terms of safety and reliability must be ensured. Also, the location of the case study, in a coastal city, where the saline and humid nature of the weather, worsened by climate-change-related intense events, might seriously compromise a satisfactory level of setting within a reasonable amount of time, and durability could be challenging, made clear that a controlled use of hydraulic lime shall be opted for. In this framework, NHL 3.5 was preferred to provide the fresh mortar with the minimum early-setting capacity, enabling the implementation of a complete and fully working potential



**Figure 9.** Preparation of samples in the laboratory - penetrometer test to estimate of the compressive strength of samples - porosity accessible to water and bulk density through the hydrostatic balance method.

consolidation intervention. Furthermore, as the hydraulic lime mortar gains strength in time, it was considered to test specimens at 60 days so that most of the strength increase had already occurred. Finally, a limited percentage (5%) of calcite sand, which is known to promote strength gain during setting, was employed (Lanas and Alvarez-Galindo 2003; Lanas et al. 2004; Matias, Torres, and Faria 2016; Silva, Ferreira Pinto, and Gomes 2014).

A binder/aggregate ratio of 1.5 was assumed. The selected aggregate was composed predominantly of quartz, micas, feldspars, and a limited amount of calcite (5% of the total sand employed). Crushed brick powder (cocciopesto) with a maximum grain size of 0.18 mm was added up to 50% of the aggregate quantity, ensuring not only similarity in composition but also in the appearance characterized by the red of the cocciopesto. Aggregate granulometry was selected to obtain a curve as close as possible to the historical one; Figure 10 and Table 5 show the results of the analysis carried out on the aggregate of Mix-1, including the uniformity and curvature coefficients,  $c_u$  and  $c_c$ , respectively. The water added to the dry mixture was 26% of the weight. Overall, the mix design ensured similarity between historical and new mortar in terms of mineralogical composition and grain size.

Nine specimens with dimensions of  $40 \times 40 \times 160 \text{ mm}^3$  were prepared with Mix-1. All the tests on mortars were carried out at 60-days age of the specimens. Three specimens were employed to perform penetrometer tests to estimate the compressive strength and evaluate open porosity through the hydrostatic balance test. Penetrometer tests on the specimens of the repair mortar Mix-1 provided an average strength  $\sigma_{r,Mix-1}^p = 3.8 \text{ Mpa}$ . The average value refers to three acceptable measuring points and shows a coefficient of variation  $CV = 24\%$ . For open porosity, results provided an average value of  $P_{r,Mix-1} = 34.65\%$ ; the average value refers to five acceptable tests and shows a coefficient of variation  $CV = 19\%$ , so porosity ranges between  $34\% \pm 6.58\%$ . Three specimens with dimensions  $40 \times 40 \times 160 \text{ mm}^3$  were subjected to linear thermal expansion coefficient test grounding on the alternative method foreseen in (EN1770 2000) where measurements are carried out sequentially at sample temperatures of  $-20, 0^\circ\text{C}, 200\text{C}, 400\text{C},$  and  $600\text{C}$ .

Results provided an average value of the thermal expansion coefficient in the range  $-20\text{C}/40\text{C}$  equal to  $\alpha_{-20/40} = 8.46 \times 10^{-6} \text{ C}^{-1}$  and a related C.o.V. of 3.34%, consistently with the literature results on similar admixtures (Černý et al. 2006; Van Balen et al. 2007).

To gain complete characterization, three specimens with dimensions  $40 \times 40 \times 160 \text{ mm}^3$  were subjected to three-point bending and compression tests on the prism halves according to (EN1015–11 2019). Results provided an average bending strength  $\sigma_{b,t} = 1.13 \text{ MPa}$  and  $\text{CV} = 29\%$  and an average compressive strength  $\sigma_c = 3.02 \text{ MPa}$  and  $\text{CV} = 13\%$ .

Given the results on the historical mortar reported before, the acceptance ranges become:

$$\begin{aligned} 34.1\% \leq P_r &\leq 40.3\% \\ 4.16 \text{ MPa} \leq \sigma_r &\leq 5.2 \text{ MPa} \end{aligned} \quad (2)$$

The experimental results on Mix-1 indicated that the porosity met the acceptance criteria, being  $P_{r,Mix-1} = 34.65\%$ , but the strength does not fall within the acceptable ranges, having too low a value ( $\sigma_{r,Mix-1}^p = 3.8 \text{ MPa}$ ). Consequently, a new formulation, referred to as Mix-2, was developed.

## 6.2. Mix-2

To enhance strength of Mix-2 compared to Mix-1, the amount of aggregate was decreased by 10%, considering a 1.7 b/a ratio, while the water was changed from 26% to 29% of the weight. Mix-2 mortar samples were subjected to the same tests as Mix-1, and the results indicate that the Mix-2 properties are within the acceptable range for both parameters. In particular, porosity  $P_{r,Mix-2} = 35.2\%$ . Concerning compressive strength, penetrometer test results provided  $\sigma_{r,Mix-2}^p = 4.3 \text{ MPa}$ , which is lower than the upper threshold, i.e.,  $\sigma_h = 5.2 \text{ MPa}$ . Results of penetrometer tests and porosity for Mix-1 and Mix-2 are reported in Table 4. As an additional test to characterize the mortar, three-point bending and compression tests were also implemented on Mix-2. Results provided an average bending strength  $\sigma_{b,t} = 0.99 \text{ MPa}$  and  $\text{CV} = 16\%$  and an average compressive strength  $\sigma_c = 3.4 \text{ MPa}$  and  $\text{CV} = 8\%$ .

## 6.3. Validation of the procedure

Further analyses were performed to evaluate the effectiveness of the proposed procedure. In particular, DIA of the new mixes was performed to compare results with the known composition and grain size data. Furthermore, the direct comparison between the results of DIA obtained from the C<sub>1</sub> and C<sub>3</sub> samples of historical mortar and those from Mix-1 and Mix-2 permitted further examination of historical and new mortar compatibility factors.

DIA on the thin section samples of the new mixes, TS-Mix-1 and TS-Mix-2, was implemented with the same procedure described above. Colored images

with crossed and parallel Nicols frames were taken with pixel dimensions  $19,516 \times 12,024$  and  $19,113 \times 10,158$  for Mix-1 and Mix-2, respectively, with a resolution of 150 DPI in TIFF format.

Figure 10 and Table 5 compare the grain size curves determined through DIA for the specimens of historical and new mortars, as well as the curve obtained by sieving the aggregate employed to prepare the new mortar specimens. As mentioned, original mortars, DIA-C1 and DIA-C2, show similar curves. Furthermore, comparing the actual granulometric curve and those deduced through DIA for Mix-1 and Mix-2, it is clear that DIA overestimates the fine fraction (between 0.125 mm and 0.5 mm) while coarser grains are not tackled entirely, see Table 5. The overestimation, which is around 15% for the fine fraction (0.063 mm), and then reduced for the larger classes, can be related to both segmentation errors and the thin section effect, which alters the amount occupied by the grains since they are cut at a height that is unavoidably different from the maximum-diameter plane height. The contrast and brightness thresholds selected affect the overestimation related to the segmentation process. This can lead to mistakenly associating certain regions of the binder as aggregate or vice-versa. This phenomenon appears, in this case, less marked for medium-sized gains. This result is in line with previous results available in the literature Mertens and Elsen (2006); Sitzia, Beltrame, and Mirão (2022); Piovesan, Mazzoli, and Maritan (2023); Carò and Di Giulio (2004); Middendorf, Schade, and Kraus (2019); Chong et al. (2021); Marinoni et al. (2005). Using multiple images and thin sections of the same mortar can limit this error, providing statistical robustness.

Furthermore, the uniformity coefficient,  $c_u$ , and the curvature coefficient,  $c_c$ , were evaluated for all the curves of Figure 10 considering,  $c_u = d_{60}/d_{10}$  and  $c_c = d_{30}^2/(d_{60}d_{10})$ , where,  $d_x$  is the grain size corresponding to x% passing. It is known that sand is

**Table 4.** Physical parameters and compressive strength estimated through penetrometer for Mix-1 and Mix-2; CV is the coefficient of variation, and  $n$  stands for the number of tested specimens.

		Bulk density [g/cm <sup>3</sup> ]	$P_r$ [%]	$\sigma_r^p$ [MPa]
3*Mix-1	Average	1.82	34.65	3.8
	CV [%]	12	19	27
	$n$	6	6	3
3*Mix-2	Average	1.84	35.2	4.3
	CV [%]	19	19	21
	$n$	6	6	3

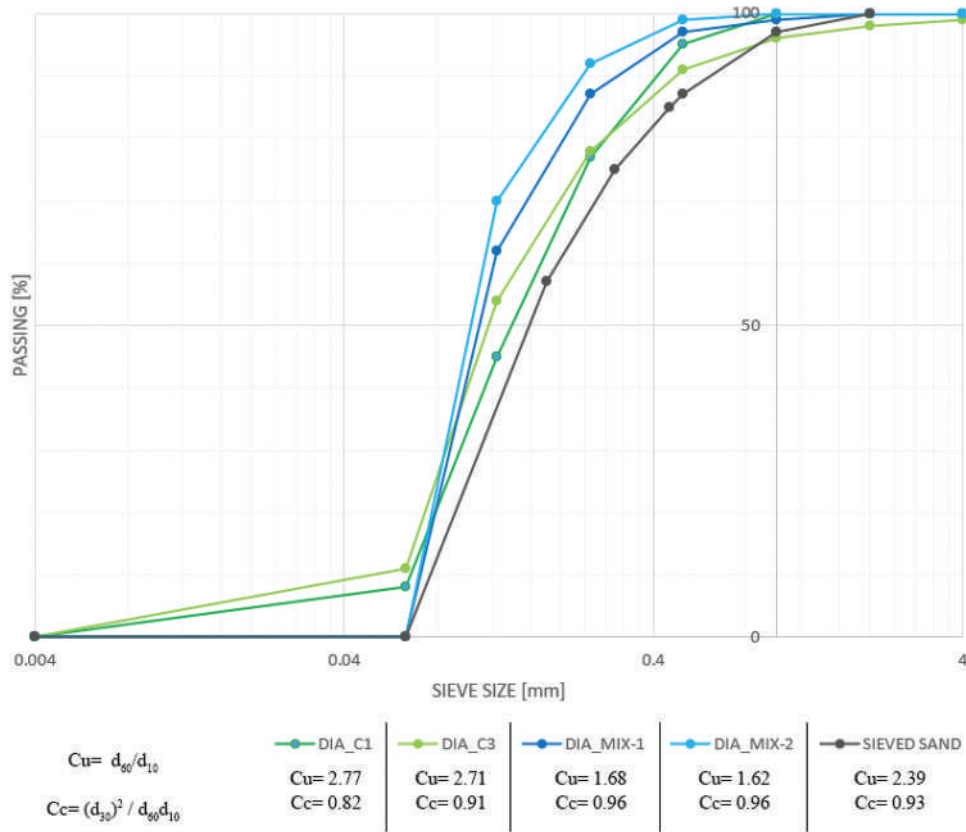


Figure 10. Comparison of estimated and used grain size curves and related coefficients of uniformity and curvature.

Table 5. Retained percentage of aggregate: estimation comparison.  $c_u$  and  $c_c$  are the coefficients of uniformity and curvature, respectively (Figure 10).

[mm]	DIA-C <sub>1</sub>	DIA-C <sub>3</sub>	DIA-MIX-1	DIA-MIX-2	[mm]	new mix sieved
4	-	1	-	-	2	-
2	-	1	-	-	1	3
1	-	2	1	-	0.5	10
0.5	5	5	2	1	0.45	2
0.25	18	13	10	7	0.3	10
0.125	32	24	25	22	0.18	18
0.063	37	43	62	70	0.063	57
0.004	8	11	-	-	0.004	-

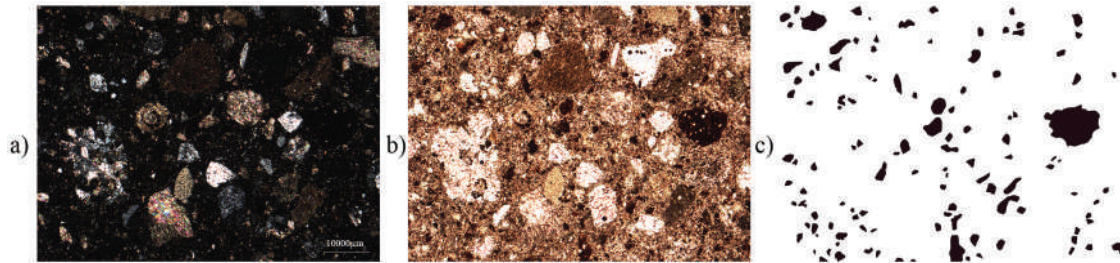
considered well-graded if  $c_u \geq 6$  and  $1 \leq c_c \leq 3$ , out of these ranges, soil is considered poorly graded, indicating substantially a narrow range of particle sizes and a too steep inclination of the grading curve. A higher value of  $c_u$  signifies that the grains can interlock more effectively, providing strength and stability. The values of the  $c_c$  indicate, in all the cases, an imbalance in the particle distribution, with the predominance of coarser grains, poor mixture stability, and, eventually, durability. The range showed by these grains is classified as open-graded, differently from ideal layout, i.e., dense graded to reach maximum packing density (Kalore and Sivakumar Babu 2023),.

Table 6 shows the estimates of the amount of surface void-content deduced from DIA for both historical and new mixes. These values are clearly not comparable with the open porosity determined experimentally because of the same thin-section effect, which partially jeopardizes the analyses of the grain size, reading in the 2D surface a 3D phenomenon. Hence, DIA should be complemented with other methods to determine porosity. Nonetheless, the results of surface porosity still enable a comparative analysis that confirms uniformity among all samples. Table 6 also compares the data on the b/a ratio estimated through DIA and employed in the realization of the samples and shows good agreement, confirming the procedure’s reliability.

To analyse the presence of cocciopesto, two restricted portions of the thin sections TS-C<sub>1</sub> and TS-Mix-2 were considered and compared (see Figures 8 and 11). Manual segmentation is performed employing the already mentioned threshold values. In the TS-C<sub>1</sub>, the percentage of cocciopesto on the total area was found to equal 13%, around a third of the aggregate. As for TS-Mix-2, cocciopesto was found to equal 11% of the total surface, while in reality, 20% of cocciopesto was employed. Hence, the result shows an underestimation of the employed amount reasonably connected to the very

**Table 6.** Results of the thin section DIA for historical and new mortars and comparison with the data of used ones.

	Surface void-content [%]	Binder [%]	Aggregate [%]	b/a [-]	b/a employed [-]
TS-C <sub>1</sub>	4	61.6	38.4	1.6	
TS-C <sub>3</sub>	5	64.9	35.1	1.85	
MIX-1	3	60.8	39.2	1.55	1.5
MIX-2	4	62.7	37.3	1.68	1.7



**Figure 11.** Zoomed 5 (5x) frame from thin section analysis in transmitted-light microscope with crossed Nicols (a) and parallel Nicols (b) for specimen TS-Mix-2 identifying the cocchiopesto (c).

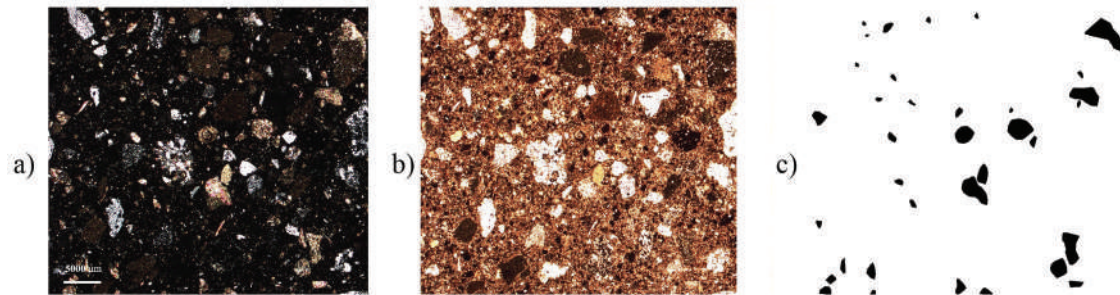


**Figure 12.** Zoomed image (2.5X) frame from thin section analysis in transmitted-light microscope with crossed nicols (a) and parallel nicols (b) for specimen TS-Mix-2 identifying the carbonate aggregates (c).

fine dimension of the cocchiopesto grains not easily distinguishable in color.

To further enhance the data obtained from the analysis of the thin section image, a restricted portion of the thin section corresponding to TS-Mix-2 was considered to analyze the nature of the aggregate. The TIFF image is  $2080 \times 1540$  pixels, with a resolution of 150 DPI. Manual segmentation employed threshold values equal to (90–255), see Figure 12. Indeed, due to the different colors resulting from birefringence, it is possible to distinguish silicate-type aggregates from carbonate aggregates in a thin section. In particular, carbonate rocks tend toward a pinkish hue compared to quartz, for instance, which will tend toward white. For the area considered by DIA, the percentage of carbonate aggregate was found to equal 2.2% of the total surface area. In the mix preparation, 5% of the aggregate employed was

calcite sand, 1.95% of the total, hence providing satisfactory estimation considering the percentage searched is remarkably little.

## 7. Conclusions

In this study, a procedure that provides quantitative indicators to support the design of repair mortars compatible with the original historical ones is presented. The procedure employs laboratory and on-site characterization tests and Digital Image Analysis (DIA) of thin sections in a polarized-light microscope. An Ottoman military building, the Casemates in the Casbah of Algiers, is considered as a case study. Results show that:

- The analyzed historical mortar is very rich in binder and shows no lime lumps, indicating care in the

production process, although shrinkage fractures were highlighted by DIA;

- Porosity and strength values are similar to other studies on monumental buildings in the Mediterranean area;
- Coarse grain additives promoting hydraulicity (*cocciopesto*), were found;
- The granulometric curve extrapolated through DIA shows a predominance of coarser grains, meaning open-graded sand with loose packing density;

On the newly designed mixes, for which the composition was known, it was possible to validate the procedure based on DIA, suggesting that:

- DIA method provides reliable and relatively rapid results of the b/a ratio, although the complete identification of aggregates may not be systematic. Nevertheless, the observed margin of error remains low and broadly acceptable, thus validating this method.
- In the identification of grain size distribution, DIA can accumulate errors due to the segmentation process and the effect of thin-section cutting. The use of multiple images may provide added robustness.
- The percentage of carbonate aggregates could be identified through DIA, although with acceptable errors, because of the birefringence properties of crystals. This type of result could be challenging to retrieve with other methodologies, especially because of the limited amount of original mortars available.
- Finer *cocciopesto* particles, of which the new mixes were rich, were more challenging to detect than coarser ones, which often represent the predominant size in historical mortars.

## Disclosure statement

No potential conflict of interest was reported by the author(s).

## References

- Abderrahim Mahindad, N. 2017. Les différents systèmes constructifs et l'évolution des caractéristiques des matériaux archéologiques du XIII<sup>ème</sup> au XVII<sup>ème</sup> siècle en Algérie. PhD diss., Université M'Hamed Bougara: Faculté des sciences de l'ingénieur.
- Aggelakopoulou, E., E. Ksinopoulou, and V. Eleftheriou. 2022. Evaluation of mortar mix designs for the conservation of the acropolis monuments. *Journal of Cultural Heritage* 55:300–08. doi: [10.1016/j.culher.2022.04.004](https://doi.org/10.1016/j.culher.2022.04.004).
- Ali, A., Y. W. Chiang, and R. M. Santos. 2022. X-ray diffraction techniques for mineral characterization: A review for engineers of the fundamentals, applications, and research directions. *Minerals* 12 (2):205. doi: [10.3390/min12020205](https://doi.org/10.3390/min12020205).
- Apostolopoulou, M., E. Aggelakopoulou, A. Bakolas, and A. Moropoulou. 2018. Compatible mortars for the sustainable conservation of stone in masonries. *Advanced Materials for the Conservation of Stone* 97–123.
- Apostolopoulou, M., P. G. Asteris, D. J. Armaghani, M. G. Douvika, P. B. Lourenço, L. Cavaleri, A. Bakolas, and A. Moropoulou. 2020. Mapping and holistic design of natural hydraulic lime mortars. *Cement and Concrete Research* 136:106167. doi: [10.1016/j.cemconres.2020.106167](https://doi.org/10.1016/j.cemconres.2020.106167).
- Arizzi, A., and G. Cultrone. 2021. Mortars and plasters—how to characterise hydraulic mortars. *Archaeological and Anthropological Sciences* 13 (9):144.
- Avdelidis, N. P., and A. Moropoulou. 2004. Applications of infrared thermography for the investigation of historic structures. *Journal of Cultural Heritage* 5 (1):119–27.
- Baccaro, M. L. P., S. Balzi, L. Del Chiaro, and S. Vannucci. 2000. The effects of the strong use of cements in restoration: The case of Barga Duomo (northern Tuscany). Proceedings of the 9th International Congress on deterioration and conservation of stone. Venice, Italy, vol. 2, 19–24.
- Barsottelli, M., F. Fratini, P. Giovannini, and C. Manganeli Del Fà. 1998. Transport of fluids in the plaster-masonry system. In *PACT*, 127–7. Strasbourg, France: Conseil de l'Europe.
- Beck, K., and M. Al-Mukhtar. 2008. Formulation and characterization of an appropriate lime-based mortar for use with a porous limestone. *Environmental Geology* 56 (3):715–27. doi: [10.1007/s00254-008-1299-8](https://doi.org/10.1007/s00254-008-1299-8).
- Bekzhanova, Z., S. Ali Memon, and J. Ryeol Kim. 2021. Self-sensing cementitious composites: Review and perspective. *Nanomaterials: Overview and Historical Perspectives* 11 (9):2355.
- Benedetti, A., and M. Tarozzi. 2020. Interpretation formulas for in situ characterization of mortar strength. *Construction and Building Materials* 242:118093. <https://doi.org/10.1016/j.conbuildmat.2020.118093>
- Bertolin, C., and A. Loli. 2018. Sustainable interventions in historic buildings: A developing decision making tool. *Journal of Cultural Heritage* 34:291–302. doi: [10.1016/j.culher.2018.08.010](https://doi.org/10.1016/j.culher.2018.08.010).
- Birgin, H. B., A. D'Alessandro, S. Laflamme, and F. Ubertini. 2021. Hybrid carbon microfibers-graphite fillers for piezoresistive cementitious composites. *Sensors (Switzerland)* 21 (2):518.
- Blaeuer, C., and A. Kueng. 2007. Examples of microscopic analysis of historic mortars by means of polarising light microscopy of dispersions and thin sections. *Materials Characterization* 58 (11–12):1199–207.
- Bocca, P., and A. Grazzini. 2012. Experimental procedure for the prequalification of strengthening mortars. *International Journal of Architectural Heritage* 6 (3):302–21.
- Bocca, P., and A. Grazzini. 2013. Mechanical properties and freeze-thaw durability of strengthening mortars. *Journal of Materials in Civil Engineering* 25 (2):274–80. doi: [10.1061/\(ASCE\)MT.1943-5533.0000597](https://doi.org/10.1061/(ASCE)MT.1943-5533.0000597).

- Borsoi, G., A. Santos Silva, P. Menezes, A. Candeias, and J. Mirão. 2019. Analytical characterization of ancient mortars from the archaeological roman site of pisões (beja, Portugal). *Construction and Building Materials* 204:597–608. doi: [10.1016/j.conbuildmat.2019.01.233](https://doi.org/10.1016/j.conbuildmat.2019.01.233).
- Bracciale, M. P., S. Sammut, J. Cassar, M. Laura Santarelli, and A. Marrocchi. 2020. Molecular crystallization inhibitors for salt damage control in porous materials: An overview. *Molecules* 25 (8):1873. doi: [10.3390/molecules25081873](https://doi.org/10.3390/molecules25081873).
- Bunaciu, A. A., E. G. Udriștioiu, and H. Y. Aboul-Enein. 2015. X-ray diffraction: Instrumentation and applications. *Critical Reviews in Analytical Chemistry* 45 (4):289–99.
- Buresi, P., M. Ghouirgate, P. Bourmaud, F. Hitzel, C. Lefèvre, R. Madinier, and M. Oualdi. 2018. *Histoire des pays d’Islam: De 1453 à nos jours*. Paris, France: Armand Colin.
- Carò, F., and A. Di Giulio. 2004. Reliability of textural analysis of ancient plasters and mortars through automated image analysis. *Materials Characterization* 53 (2–4):243–57.
- Carpinteri, A., L. Dimastrogiovanni, and N. Pugno. 2004. RILEM recommendation MDT. D. 1—indirect determination of the surface strength of unweathered hydraulic cement mortar by the drill energy method. *Materials and Structures* 37 (7):485–87.
- Cazalla Vázquez, O. 2002. Morteros de cal: aplicación en el patrimonio histórico, Universidad de Granada. *Journal*.
- Černý, R., A. Kunca, V. Tydlitát, J. Drchalová, and P. Rovnaníková. 2006. Effect of pozzolanic admixtures on mechanical, thermal and hygric properties of lime plasters. *Construction and Building Materials* 20 (10):849–57. doi: [10.1016/j.conbuildmat.2005.07.002](https://doi.org/10.1016/j.conbuildmat.2005.07.002).
- Charter, V. 1964. *International charter for the conservation and restoration of monuments and sites*. Venice, Italy: ICOMOS.
- Chen, Z., H. Liu, L. Xu, and W. Ge. 2024. A review of mechanical properties and carbonation behavior evolution of lime mortar for architectural heritages restoration. *Minerals and Mineral Materials* 3 (1). doi: [10.20517/mmm.2023.26](https://doi.org/10.20517/mmm.2023.26).
- Chong, W., R. Othman, R. Putra Jaya, D. Shu Ing, X. Li, M. H. Wan Ibrahim, M. M. A. B. Abdullah, A. V. Sandu, B. Płoszaj, J. Szmidla, et al. 2021. Image analysis of surface porosity mortar containing processed spent bleaching earth. *Materials* 14 (7):1658. <https://doi.org/10.3390/ma14071658>
- Cnudde, V., M. Dierick, J. Vlassenbroeck, B. Masschaele, E. Lehmann, P. Jacobs, and L. Van Hoorebeke. 2008. High-speed neutron radiography for monitoring the water absorption by capillarity in porous materials. *Nuclear Instruments & Methods in Physics Research: Section B, Beam Interactions with Materials & Atoms* 266 (1):155–63. doi: [10.1016/j.nimb.2007.10.030](https://doi.org/10.1016/j.nimb.2007.10.030).
- Columbu, S., F. Sitzia, and G. Verdiani. 2015. Contribution of petrophysical analysis and 3D digital survey in the archaeometric investigations of the Emperor Hadrian’s baths (tivoli, Italy). *Rendiconti Lincei* 26 (4):455–74. doi: [10.1007/s12210-015-0469-3](https://doi.org/10.1007/s12210-015-0469-3).
- Columbu, S., M. Usai, C. Rispoli, and D. Fancello. 2022. Lime and cement plasters from 20th Century buildings: Raw materials and relations between mineralogical–petrographic characteristics and chemical–physical compatibility with the limestone substrate. *Minerals* 12 (2):226.
- Costa, D., A. Magalhães, and M. Do Rosário Veiga. 2012. Characterisation of mortars using drilling resistance measurement system (DRMS): Tests on field panels samples. In *Historic mortars: Characterisation, assessment and repair*, 413–23. Springer. [https://doi.org/10.1007/978-94-007-4635-0\\_32](https://doi.org/10.1007/978-94-007-4635-0_32)
- Costigan, A., and S. Pavia. 2009. Compressive, flexural and bond strength of brick/lime mortar masonry. *Proceedings of PROHITEC* 9 (1):1609–15.
- Dalla, P. T., I. K. Tragazikis, G. Trakakis, C. Galiotis, K. G. Dassios, and T. E. Matikas. 2021. Multifunctional cement mortars enhanced with graphene nanoplatelets and carbon nanotubes. *Sensors (Switzerland)* 21 (3):933. doi: [10.3390/s21030933](https://doi.org/10.3390/s21030933).
- Degryse, P., J. Elsen, and M. Waelkens. 2002. Study of ancient mortars from Sagalassos (Turkey) in view of their conservation. *Cement and Concrete Research* 32 (9):1457–63. doi: [10.1016/S0008-8846\(02\)00807-4](https://doi.org/10.1016/S0008-8846(02)00807-4).
- Del Mar Barbero-Barrera, M., L. Maldonado-Ramos, K. Van Balen, A. García-Santos, and F. Javier Neila-González. 2014. Lime render layers: An overview of their properties. *Journal of Cultural Heritage* 15 (3):326–30. doi: [10.1016/j.culher.2013.07.004](https://doi.org/10.1016/j.culher.2013.07.004).
- Diamond, S. 2004. The microstructure of cement paste and concrete—a visual primer. *Cement and Concrete Composites* 26 (8):919–33.
- Dimitrova, E., M.-L. Lavenir, P. McMahon, B. Mürniece, S. F. Musso, G. Nagy, C. Rauhut, G. D. Rourke, E. Sciacchitano, and B. Selfslagh. 2020. European quality principles for EU-funded interventions with potential impact upon cultural heritage. Paris, France: ICOMOS, November. <https://open.archive.icomos.org/id/eprint/2436/>: Revised.
- Do Rosario Veiga, M., A. Fragata, A. L. Velosa, A. C. Magalhães, and G. Margalha. 2010. Lime-based mortars: Viability for use as substitution renders in historical buildings. *International Journal of Architectural Heritage* 4 (2):177–95.
- Drdácký, M. F., and D. Michoinova. 2003. Lime mortars with natural fibres. In *Brittle matrix composites*, ed. A. R. Bunsell, vol. 7, 523–32. Amsterdam, Netherlands: Elsevier. <https://doi.org/10.1533/9780857093103.523>
- Drougkas, A., P. Roca, and C. Molins. 2016. Compressive strength and elasticity of pure lime mortar masonry. *Materials and Structures* 49 (3):983–99. doi: [10.1617/s11527-015-0553-2](https://doi.org/10.1617/s11527-015-0553-2).
- Drougkas, A., V. Sarhosis, M. Basheer, A. D’Alessandro, and F. Ubertini. 2023. Design of a smart lime mortar with conductive micro and nano fillers for structural health monitoring. *Construction and Building Materials* 367:130024. <https://doi.org/10.1016/j.conbuildmat.2022.130024>
- Drougkas, A., V. Sarhosis, A. Macente, M. Basheer, A. D’Alessandro, and F. Ubertini. 2023. Mechanical and durability testing and XCT imaging of a lime-based micro-scale modified smart intervention mortar. *International Journal of Architectural Heritage* 19 (2):276–91. <https://doi.org/10.1080/15583058.2023.2278067>
- Elert, K., C. Rodriguez-Navarro, E. Sebastian Pardo, E. Hansen, and O. Cazalla. 2002. Lime mortars for the conservation of historic buildings. *Studies in Conservation* 47 (1):62–75.

- EN1015-11. 2019. Methods of test for mortar for masonry-part 3: Determination of flexural and compressive strength of hardened mortar. CEN.
- EN12390-13. 2021. Testing hardened concrete - Part 13: Determination of secant modulus of elasticity in compression. CEN.
- EN1770. 2000. Products and systems for the protection and repair of concrete structures - test methods - determination of the coefficient of thermal expansion. CEN.
- Faria, P., P. Duarte, D. Barbosa, and I. Ferreira. 2017. New composite of natural hydraulic lime mortar with graphene oxide. *Construction and Building Materials* 156:1150–57. <https://doi.org/10.1016/j.conbuildmat.2017.09.072>
- Fazzi, E., G. Misseri, and L. Rovero. 2023. Influence of matrix and cohesive material law characteristics on the tensile and bond behavior of FRMC systems. *Journal of Composites for Construction* 27 (5):04023048.
- Feo, L., R. Luciano, G. Misseri, and L. Rovero. 2016. Irregular stone masonries: Analysis and strengthening with glass fibre reinforced composites. *Composites Part B Engineering* 92:84–93. doi: [10.1016/j.compositesb.2016.02.038](https://doi.org/10.1016/j.compositesb.2016.02.038).
- Fontaine, L., M. L. Thomson, and G. T. Suter. 1999. Practice and research: The need for standards for historic mortars. In *The use of and need for preservation standards in architectural conservation*, 158–71. ASTM International. <https://doi.org/10.1520/STP14190S>
- Gaid, M. 1990. *L'Algérie sous les Turcs*, 236. Mimouni. Alger, Algérie.
- Garijo, L., X. Zhang, G. Ruiz, J. J. Ortega, and C. Yu Rena. 2017. Advanced mechanical characterization of NHL mortars and cohesive simulation of their failure behavior. *Construction and Building Materials* 153:569–77.
- Ghabezloo, S. 2011. Micromechanics analysis of thermal expansion and thermal pressurization of a hardened cement paste. *Cement and Concrete Research* 41 (5):520–32. doi: [10.1016/j.cemconres.2011.01.023](https://doi.org/10.1016/j.cemconres.2011.01.023).
- Gleize, P. J. P., A. Müller, and H. R. Roman. 2003. Microstructural investigation of a silica fume–cement–lime mortar. *Cement and Concrete Composites* 25 (2):171–75.
- Gomes, O. D. F. M., P. Roberto Lopes Lima, and A. Vianna Fontes. 2012. Morphological characterization of natural and artificial sands through image analysis. *Proceedings of the 10th International Congress for Applied Mineralogy (ICAM)* Springer, 255–63. [https://doi.org/10.1007/978-3-642-27682-8\\_32](https://doi.org/10.1007/978-3-642-27682-8_32)
- Grammatikakis, G., K. D. Demadis, K. Melessanaki, and P. Pouli. 2015. Laser-assisted removal of dark cement crusts from mineral gypsum (selenite) architectural elements of peripheral monuments at Knossos. *Studies in Conservation* 60 (sup1):S3–11. doi: [10.1179/0039363015Z.000000000201](https://doi.org/10.1179/0039363015Z.000000000201).
- Granneman, S. J., B. Lubelli, and R. P. van Hees. 2019a. Effect of mixed in crystallization modifiers on the resistance of lime mortar against NaCl and Na<sub>2</sub>SO<sub>4</sub> crystallization. *Construction and Building Materials* 194:62–70.
- Groot, C., G. Ashall, and J. Hughes. 2007. Report 28: Characterisation of old mortars with respect to their repair-state-of-the-art report of RILEM technical committee 167-COM. RILEM publications.
- Groot, C., R. Veiga, I. Papayianni, R. Van Hees, M. Secco, J. I. Alvarez, P. Faria, and M. Stefanidou. 2022. RILEM TC 277-LHS report: Lime-based mortars for restoration—a review on long-term durability aspects and experience from practice. *Materials and Structures* 55 (10):245. doi: [10.1617/s11527-022-02052-1](https://doi.org/10.1617/s11527-022-02052-1).
- Gucci, N., and R. Barsotti. 1995. A non-destructive technique for the determination of mortar load capacity in situ. *Materials and Structures* 28:276–83.
- Heikal, M., H. El-Didamony, and M. S. Morsy. 2000. Limestone-filled pozzolanic cement. *Cement and Concrete Research* 30 (11):1827–34.
- Henriques, F. M. 2005. Challenges and perspectives of replacement mortars in architectural conservation. International workshop. Repair mortars for historic masonry, Rilem technical Committee, 26–28, TU Delft.
- Houck, J., and G. W. Scherer. 2006. Controlling stress from salt crystallization. In *Natural stone, weathering phenomena, conservation strategies and case studies*, ed. S. Siegesmund, T. Weiss, and A. Vollbrecht, 299–312. Geological Society of London. <https://doi.org/10.1144/GSL.SP.2006.271.01.25>
- Hover, K. C. 2011. The influence of water on the performance of concrete. *Construction and Building Materials* 25 (7):3003–13.
- ICOMOS. 2003. Principles for the analysis, conservation and structural restoration of architectural heritage. Proceedings of the ICOMOS 14th General Assembly in Victoria Falls, 27–31, Victoria Falls, Zimbabwe.
- Icomos, I. 2001. Recommendations for the analysis, conservation and structural restoration of architectural heritage. Icomos International Scientific Committee for Analysis and Restoration of Structures of Architectural Heritage, Victoria Falls, Zimbabwe.
- Iscarsah, I. C. O. M. O. S. 2005. Recommendations for the analysis, conservation and structural restoration of architectural heritage. *Icomos International Scientific Committee For Analysis and Restoration of Structures of Architectural Heritage*.
- ISO113578. 2021. Plastics — differential scanning calorimetry (DSC) part 8: Determination of thermal conductivity. ISO.
- ISO20290-1. 2021. Aggregates for concrete — test methods for mechanical and physical properties part 1: Determination of bulk density, particle density, particle mass-per-volume and water absorption. ISO.
- Kaklis, K. N., S. P. Maurigiannakis, Z. G. Agioutantis, and P. Maravelaki-Kalaitzaki. 2018. Characterization of pozzolanic lime mortars used as filling material in shaped grooves for restoring member connections in ancient monuments. *International Journal of Architectural Heritage* 12 (1):75–90.
- Kalagri, A., I. Karatasios, and V. Kilikoglou. 2014. The effect of aggregate size and type of binder on microstructure and mechanical properties of NHL mortars. *Construction and Building Materials* 53:467–74.
- Kalore, S. A., and G. L. Sivakumar Babu. 2023. Significance of Cu and cc in evaluating internal stability with application to design of subbase gradation in pavements. *Transportation Geotechnics* 40:100972. doi: [10.1016/j.trgeo.2023.100972](https://doi.org/10.1016/j.trgeo.2023.100972).
- Karagiannis, N., M. Karoglou, A. Bakolas, and A. Moropoulou. 2016. Building materials capillary rise coefficient: Concepts, determination and parameters

- involved. *New Approaches to Building Pathology and Durability* 27–44. [https://doi.org/10.1007/978-981-10-0648-7\\_2](https://doi.org/10.1007/978-981-10-0648-7_2)
- Klug, H. P., L. E. Alexander, O. P. Bertini, and A. Negro. 1969. *Diffrazione dei raggi X: metodi per le sostanze policristalline e amorfe*. Turin, Italy: Albra.
- Kumar, D. N., and P. R. Kumar. 2022. Investigations on alternate lime-pozzolana based mortars for repair of heritage structures. *Construction and Building Materials* 341:127776.
- Kwame, O. S. 2008. Assessment of the coefficient of thermal expansion of alabama concrete. PhD diss. master's thesis, USA: Auburn University.
- Lanas, J., and J. I. Alvarez-Galindo. 2003. Masonry repair lime-based mortars: Factors affecting the mechanical behavior. *Cement and Concrete Research* 33 (11):1867–76.
- Lanas, J., M. Arandigoyen, J. I. Alvarez, J. L. Pérez Bernal, and M. Angel Bello. 2004. Mechanical behavior of masonry repair mortars: Aerial and hydraulic lime-based mixtures. *10th International Congress on Deterioration and Conservation of Stones Stockholm 2*, 1–16.
- Lanas, J., J. L. Pérez Bernal, M. A. Bello, and J. I. Alvarez Galindo. 2004. Mechanical properties of natural hydraulic lime-based mortars. *Cement and Concrete Research* 34 (12):2191–201.
- Lanzón, M., and P. A. García-Ruiz. 2009. Evaluation of capillary water absorption in rendering mortars made with powdered waterproofing additives. *Construction and Building Materials* 23 (10):3287–91.
- Levioldi, S., and A. G. Fabbri. 1986. Image processing in Italy: A first report. In *Image analysis and processing*, 259–67. Boston, MA: Springer. [https://doi.org/10.1007/978-1-4613-2239-9\\_29](https://doi.org/10.1007/978-1-4613-2239-9_29)
- Loke, M. E., P. Kumar, and G. Cultrone. 2023. Challenges in characterization and development of suitable historic repair mortars. *International Journal of Conservation Science* 14 (3). 783–802.
- Loureiro, A. M. S., S. P. Paz, M. Do Rosário Veiga, and R. Angélica. 2020. Assessment of compatibility between historic mortars and lime-metakaolin restoration mortars made from amazon industrial waste. *Applied Clay Science* 198:105843. <https://doi.org/10.1016/j.clay.2020.105843>
- Luque, A., G. Cultrone, and E. Sebastián. 2010. The use of lime mortars in restoration work on architectural heritage. *Materials, Technologies and Practice in Historic Heritage Structures* 3-11, 197–207.
- Marastoni, D., A. Benedetti, L. Pelá, and G. Pignagnoli. 2017. Torque penetrometric test for the in-situ characterisation of historical mortars: Fracture mechanics interpretation and experimental validation. *Construction and Building Materials* 157:509–20. doi: [10.1016/j.conbuildmat.2017.09.120](https://doi.org/10.1016/j.conbuildmat.2017.09.120).
- Marinoni, N., A. Pavese, M. Foi, and L. Trombino. 2005. Characterisation of mortar morphology in thin sections by digital image processing. *Cement and Concrete Research* 35 (8):1613–19. doi: [10.1016/j.cemconres.2004.09.015](https://doi.org/10.1016/j.cemconres.2004.09.015).
- Matias, G., I. Torres, and P. Faria. 2016. Air lime and natural hydraulic lime mortars with ceramic residues for rehabilitation of old buildings. *Proceedings of the 41st IAHS WORLD CONGRESS, Sustainability and Innovation for the Future*, Albufeira, Algarve, Portugal.
- Mechling, J.-M., and M. Baquet. 2022. Physicochemical characterisation of the mortars from Notre-Dame de Paris cathedral—preliminary findings and reconstitution of the fresh mix. *Journal of Cultural Heritage* 65 1–11. <https://doi.org/10.1016/j.culher.2022.10.006>
- Mendoza, F., and R. Lu. 2015. Basics of image analysis. *Hyperspectral Imaging Technology in Food and Agriculture* 9–56. <https://doi.org/10.1007/978-1-4939-2836-1>
- Mertens, G., and J. Elsen. 2006. Use of computer assisted image analysis for the determination of the grain-size distribution of sands used in mortars. *Cement and Concrete Research* 36 (8):1453–59. doi: [10.1016/j.cemconres.2006.03.004](https://doi.org/10.1016/j.cemconres.2006.03.004).
- Middendorf, B., T. Schade, and K. Kraus. 2019. Quantitative analysis of historic mortars by digital image analysis of thin sections. *Restoration of Buildings and Monuments* 23 (2):83–92.
- Misseri, G., L. Rovero, and S. Galassi. 2021. Analytical modelling bond behaviour of polybenzoxazole (PBO) and glass fibre reinforced cementitious matrix (FRCM) systems coupled with cement and gypsum matrixes: Effect of the cohesive material law (CML) shape. *Composites Part B Engineering* 223:109090. <https://doi.org/10.1016/j.compositesb.2021.109090>
- Moropoulou, A., A. Bakolas, and K. Bisbikou. 2000. Investigation of the technology of historic mortars. *Journal of Cultural Heritage* 1 (1):45–58.
- Moropoulou, A., A. Bakolas, P. Moundoulas, E. Aggelakopoulou, and S. Anagnostopoulou. 2005. Strength development and lime reaction in mortars for repairing historic masonries. *Cement and Concrete Composites* 27 (2):289–94.
- Moropoulou, A., K. C. Labropoulos, E. T. Delegou, M. Karoglou, and A. Bakolas. 2013. Non-destructive techniques as a tool for the protection of built cultural heritage. *Construction and Building Materials* 48:1222–39. doi: [10.1016/j.conbuildmat.2013.03.044](https://doi.org/10.1016/j.conbuildmat.2013.03.044).
- Noguchi, T., F. Tomosawa, K. M. Nemati, B. M. Chiaia, and A. P. Fantilli. 2009. A practical equation for elastic modulus of concrete. *ACI Structural Journal* 106 (5):690.
- Nogueira, R., A. Paula Ferreira Pinto, and A. Gomes. 2018. Design and behavior of traditional lime-based plasters and renders. Review and critical appraisal of strengths and weaknesses. *Cement and Concrete Composites* 89:192–204.
- Papayianni, I., M. Stefanidou, P. Vasiliki, K. Stavroula, A. Fani, and S. Maria. 2019. Evaluation of lime-based mortars used for repairing the galerius palace (4th century AD) during restoration project (1994-2006). In *Proceedings of the international conference on sustainable materials systems and structures (SMSS2019): Durability, monitoring and repair of structures*, ed. A. Baričević, M. J. Rukavina, D. Damjanović, and M. Guadagnini, 660–67. Paris: RILEM Publications SARL.
- Pecchioni, E., F. Fratini, E. Cantisani, et al. 2008. *Le malte antiche e moderne tra tradizione e innovazione*. Bologna, Italy: Pátron.
- Peroni, S., et al. 1981. Lime based mortars for the repair of ancient masonry and possible substitutes. Mortars, cements and grouts used in the conservation of historic buildings. Symposium, 63–99, Rome. Accessed November 3–6, 1981.
- Philokyrou, M., I. Ioannou, and A. Iliá. 2010. Design and production of repair mortars for historic masonry taking into account the characteristics of old mortars. 2nd Historic

- Mortars Conference HMC2010 and RILEM TC 203-RHM Final Workshop, 1051–58, Prague, Czech Republic.
- Piovesan, R., C. Mazzoli, and L. Maritan. 2023. Production recipes of mortar-based materials from ancient Pompeii by quantitative image analysis approach: The microstratigraphy of plasters in the temple of Venus. *Journal of Cultural Heritage* 59:57–68.
- Reedy, C. L. 2006. Review of digital image analysis of petrographic thin sections in conservation research. *Journal of the American Institute for Conservation* 45 (2):127–46.
- Restuccia, L., A. Lopez, G. A. Ferro, D. Liberatore, and J. M. Tulliani. 2018. An investigation of the beneficial effects of adding carbon nanotubes to standard injection grout. *Fatigue & Fracture of Engineering Materials & Structures* 41 (1):119–28.
- Riccardi, M. P., M. Lezzerini, F. Carò, M. Franzini, and B. Messiga. 2007. Microtextural and microchemical studies of hydraulic ancient mortars: Two analytical approaches to understand pre-industrial technology processes. *Journal of Cultural Heritage* 8 (4):350–60.
- RILEM-TC203-RHM. 2012. Repair mortars for historic masonry: Performance requirements for renders and plasters.
- Roca, P. 2011. Restoration of historic buildings: Conservation principles and structural assessment. *International Journal of Materials and Structural Integrity* 5 (2–3):151–67. doi: 10.1504/IJMSI.2011.041932.
- Rodrigues, J. D., and A. Grossi. 2007. Indicators and ratings for the compatibility assessment of conservation actions. *Journal of Cultural Heritage* 8 (1):32–43.
- Rovero, L., S. Galassi, and G. Misseri. 2020. Experimental and analytical investigation of bond behavior in glass fiber-reinforced composites based on gypsum and cement matrices. *Composites Part B Engineering* 194:108051.
- Schafer, J., and H. K. Hilsdorf. 1993. 74. Ancient and new lime mortars—the correlation between their composition, structure and properties. Conservation of stone and other materials: proceedings of the international RILEM/UNESCO congress held at the UNESCO headquarters, 605–12, Paris.
- Schueremans, L., Ö. Cizer, E. Janssens, G. Serré, and K. Van Balen. 2011. Characterization of repair mortars for the assessment of their compatibility in restoration projects: Research and practice. *Construction and Building Materials* 25 (12):4338–50.
- Sicat, E., F. Gong, D. Zhang, and T. Ueda. 2013. Change of the coefficient of thermal expansion of mortar due to damage by freeze thaw cycles. *Journal of Advanced Concrete Technology* 11 (12):333–46.
- Siegesmund, S., L. Sousa, and C. Knell. 2018. Thermal expansion of granitoids. *Environmental Earth Sciences* 77:1–29.
- Silva, A. S., P. Adriano, A. Magalhães, J. Pires, A. Carvalho, A. João Cruz, J. Mirão, and A. Candeias. 2010. Characterization of historical mortars from Alentejo's religious buildings. *International Journal of Architectural Heritage* 4 (2):138–54.
- Silva, B. A., A. P. Ferreira Pinto, and A. Gomes. 2014. Influence of natural hydraulic lime content on the properties of aerial lime-based mortars. *Construction and Building Materials* 72:208–18.
- Sitzia, F., M. Beltrame, and J. Mirão. 2022. The particle-size distribution of concrete and mortar aggregates by image analysis. *Journal of Building Pathology and Rehabilitation* 7 (1):74.
- Soares, K., I. Torres, I. Flores-Colen, and D. Silveira. 2023. The influence of traditional substrates on the behaviour of lime mortars. *International Journal of Architectural Heritage* 19 (3), 346–369. <https://doi.org/10.1080/15583058.2023.2286503>
- Stefanidou, M., and I. Papayianni. 2005. The role of aggregates on the structure and properties of lime mortars. *Cement and Concrete Composites* 27 (9–10):914–19.
- Szemerey-Kiss, B., and Á. Török. 2017. The effects of the different curing conditions and the role of added aggregate in the strength of repair mortars. *Environmental Earth Sciences* 76 (7):1–15. doi: 10.1007/s12665-017-6597-6.
- Thomson, M. L., J. E. Lindqvist, J. Elsen, and C. J. W. P. Groot. 2004. Porosity of historic mortars. 13th international brick and block masonry conference, Amsterdam.
- Van Balen, K., I. Papayianni, R. V. Hees, L. Binda, and A. Waldum. 2005. Introduction to requirements for and functions and properties of repair mortars. *Materials and Structures* 38 (282):781–85.
- Van Balen, K., I. Papayianni, R. Van Hees, A. W. Luigia Binda, et al. 2007. Introduction to requirements for and functions of properties of repair mortars. Rilem Report 28:151. <https://doi.org/10.1007/BF02479291>
- Van Hees, R. P. J., L. Binda, I. Papayianni, and E. Toumbakari. 2004. Characterisation and damage analysis of old mortars. *Materials and Structures* 37 (9):644–48.
- Veiga, M. R., A. S. S. José Aguiar, and F. Carvalho. 2001. Methodologies for characterisation and repair of mortars of ancient buildings. Proceedings of the 3rd International Seminar Historical Constructions, 353–62, Portugal: University of Minho Guimarães.
- Veiga, M. R., A. Magalhães, and V. Bokan-Bosilikov. 2004. Capillarity tests on historic mortar samples extracted from site. Methodology and compared results. 13th international masonry conference, Amsterdam.
- Veiga, R., A. Fragata, A. Velosa, A. Magalhães, and G. Margalha. 2008. Substitution mortars for application in historical buildings exposed to the sea environment. Analysis of the viability of several types of compositions. International conference HMC 1790–1795.
- Wang, L., and F. Aslani. 2022. Self-sensing performance of cementitious composites with functional fillers at macro, micro and nano scales. *Construction and Building Materials* 314:125679.
- Zeng, Q., K. Li, T. Fen-Chong, and P. Dangla. 2012. Effect of porosity on thermal expansion coefficient of cement pastes and mortars. *Construction and Building Materials* 28 (1):468–75.
- Zerbinatti, M., S. Fasana, A. Grazzini, et al. 2018. Prove sperimentali su miscele di malte a vista: Allestimento di un atlante operativo per interventi di manutenzione, conservazione, restauro. In Reuso 2018. L'intreccio dei saperi per rispettare il passato interpretare il presente salvaguardare il futuro, vol. 1, 1015–24. Gangemi Editore.